HHS Public Access

Author manuscript

Curr Biol. Author manuscript; available in PMC 2020 September 09.

Published in final edited form as:

Curr Biol. 2019 September 09; 29(17): 2775–2789.e7. doi:10.1016/j.cub.2019.07.009.

Non-*Crh* glutamatergic neurons in Barrington's nucleus control micturition via glutamatergic afferents from the midbrain and hypothalamus

Anne M.J. Verstegen[1,6,*], **Nataliya Klymko**[2], **Lin Zhu**[3], **John C. Mathai**[2], **Reina Kobayashi**[2], **Anne Venner**[3], **Rachel A. Ross**[1,4], **Veronique G. VanderHorst**[3], **Elda Arrigoni**[3], **Joel C. Geerling**[3,5,‡], **Mark L. Zeidel**[2,‡]

[1]Division of Endocrinology, Diabetes, and Metabolism, Department of Medicine, Beth Israel Deaconess Medical Center, Harvard Medical School, 330 Brookline Ave, Boston, MA 02215, USA.

[2]Division of Nephrology, Department of Medicine, Beth Israel Deaconess Medical Center, Harvard Medical School, 330 Brookline Ave, Boston, MA 02215, USA.

[3]Department of Neurology, Beth Israel Deaconess Medical Center, Harvard Medical School, 330 Brookline Ave, Boston, MA 02215, USA.

[4]Present address: Division of Depression and Anxiety, Department of Psychiatry, McLean Hospital, Harvard Medical School, 115 Mill St, Belmont, MA 02478 and Center for Anxiety and Traumatic Stress Disorders, Department of Psychiatry, Massachusetts General Hospital, 55 Fruit St, Boston, MA 02114.

[5]Present address: Department of Neurology, University of Iowa Carver College of Medicine, 200 Hawkins Drive, Iowa City, IA 52242, USA.

[6]Lead Contact.

Summary

Lower urinary tract symptoms (LUTS) are exceptionally common and debilitating, and are likely caused or exacerbated by dysfunction of neural circuits controlling bladder function. An incomplete understanding of neural control of bladder function limits our ability to clinically address LUTS. Barrington's nucleus (Bar) provides descending control of bladder and sphincter

[*]Corresponding author. Address for reprint requests and other correspondence: Anne M.J. Verstegen, Dept. of Medicine, Beth Israel Deaconess Medical Center; Harvard Medical School, CLS-702, 3 Blackfan Circle, Boston, MA 02215 (aversteg@bidmc.harvard.edu).

AUTHOR CONTRIBUTIONS

Conceptualization: AMJV, VGV, JCG, and MLZ. Methodology: AMJV, JCG. Software: NK, JM. Validation: AMJV, NK, and JCG. Formal Analysis: AMJV, NK, LZ, EA, JCM, AV, VGV, and JCG. Investigation: AMJV, NK, LZ, RK, JCM, and JCG. Writing - Original Draft: AMJV and RAR. Writing -Review & Editing: AMJV, NK, AV, RAR, VGV, JCG, and MLZ. Visualization: AMJV, NK, LZ, and JCG. Supervision: AMJV and MLZ. Project Administration: AMJV. Funding Acquisition: MLZ.

[‡]These authors contributed equally.

DECLARATION OF INTERESTS

The authors declare no competing interests.

function, and its glutamatergic neurons expressing corticotropin releasing hormone ($Bar^{Crh/Vglut2}$) are implicated in bladder control. However, it remains unclear whether this subset of Bar neurons are necessary for voiding, and the broader circuitry providing input to this control center remains largely unknown. Here we examine the contribution to micturition behavior of $Bar^{Crh/Vglut2}$ neurons relative to the overall Bar^{Vglut2} population. First, we identify robust, excitatory synaptic input to Bar. Glutamatergic axons from the periaqueductal gray (PAG) and lateral hypothalamic area (LHA) intensely innervate and are functionally connected to Bar, and optogenetic stimulation of these axon terminals reliably provokes voiding. Similarly, optogenetic stimulation of Bar^{Vglut2} neurons triggers voiding, whereas stimulating the $Bar^{Crh/Vglut2}$ subpopulation causes bladder contraction, typically without voiding. Next, we genetically ablate either Bar^{Vglut2} or $Bar^{Crh/Vglut2}$ neurons and found that only Bar^{Vglut2} ablation replicates the profound urinary retention produced by conventional lesions in this region. Fiber photometry recordings reveal that Bar^{Vglut2} neuron activity precedes increased bladder pressure, while activity of $Bar^{Crh/Vglut2}$ is phase-delayed. Finally, deleting *Crh* from Bar neurons has no effect on voiding and related bladder physiology. Our results help identify the circuitry that modulates Bar neuron activity, and identify subtypes that may serve different roles in micturition.

eTOC blurb:

Verstegen *et al.* shine light on Barrington's nucleus, in which neuron subpopulations have distinct activity patterns important for coordinating downstream bladder control. Furthermore, they identify nodes on the pathway to activate the micturition control center, with different roles, reflex or voluntary behavior integration, for the afferent sites.

Introduction

Lower Urinary Tract Symptoms (LUTS), which include voiding, obstructive, storage and irritative symptoms, afflict millions and are especially prevalent in the elderly population. Addressing these debilitating symptoms clinically has been hampered by an incomplete understanding of the neural control of bladder function. Significant knowledge gaps remain in the cellular and synaptic circuits that control reflex and voluntary micturition (urination).

It was shown nearly a century ago that the micturition reflex persists following supracollicular or intercollicular decerebration [1–3]. The reflex was eliminated following transections of the neuroaxis at any level caudal to the so-called Pontine Micturition Center (PMC), including at the level of the spinal cord [4–6]. Hence, the reflex (non-volitional) micturition pathway does not involve forebrain structures, yet is supraspinal in origin. The PMC is highly conserved across species. It is critical for normal voiding, as was shown in cats [1, 3, 5–9], and subsequently confirmed in rats [10], and humans [11–13]. In fact, injury or inhibition of the PMC region prevents voiding and results in urinary retention. Also, both electrical and chemical (i.e. excitatory amino acids) stimulation of the PMC region evokes bladder contractions in cat and rat [14, 15]. In line with this, PET studies in humans revealed activation of a discrete dorsal pontine region during the initiation of voiding [16].

The PMC contains a population of non-catecholamine neurons that project directly from the pons to the sacral spinal cord. These neurons form a cluster referred to as Barrington's

nucleus (Bar) after F.J.F. Barrington, who first localized micturition to the pontine tegmentum using focal lesions in cats [1, 5, 6]. Bar neurons are exclusively glutamatergic (Bar^{Vglut2}), but separate subsets have been identified that co-express corticotropin releasing hormone (*Crh*) [17–20] or estrogen receptor 1-alpha (*Esr1*) [21, 22]. *Crh*-expressing Bar ($Bar^{Crh/Vglut2}$) neurons have long been used as a proxy for Bar neurons overall; in fact, prior studies have used the $Bar^{Crh/Vglut2}$ population as a 'point of entry' for functional dissection of Bar circuitry including for the identification of brain regions providing afferent inputs to Bar [20]. However, it was recently shown that $Bar^{Esr1/Vglut2}$, not $Bar^{Crh/Vglut2}$ neurons are critically involved in external urethral sphincter (EUS) relaxation and micturition behavior [21], suggesting the $Bar^{Crh/Vglut2}$ neurons may play a lesser role in micturition control than was previously thought.

With respect to afferent control of Bar, tracing studies have revealed a large number of afferent sites providing input to Bar neurons [18, 20]. Electrical or chemical stimulation in the hypothalamus enhances bladder activity with an increase of bladder pressure and an increased rate of bladder contraction [7, 23]. In addition, pharmacologic studies have shown that modulation of midbrain periaqueductal gray (PAG) circuitry can alter bladder volume threshold for micturition [24–26], suggesting that the PAG may 'gate' the activity of PMC neurons that control micturition.

Recent studies in mouse models have informed the view that Bar, in particular its *Crh* and *Esr1*-expressing neurons, comprises a key cellular brainstem node for triggering micturition [20, 21]. Both subpopulations are likely under synaptic control by upstream neurons, including those in the lateral hypothalamic area (LHA) and PAG, although functional synaptic connectivity between these proposed afferents and Bar neurons has never been established. Here, using a novel micturition assay in freely-behaving mice, we undertook a genetically-driven, functional dissection of Bar to determine the synaptic and cellular basis by which this supraspinal circuit controls micturition. In the first part of this study, we used optogenetics to investigate the role of two major micturition-related afferents, $PAG^{Vglut2\ ->\ Bar}$ and $LHA^{Vglut2\ ->\ Bar}$. We also investigated the connectivity between these afferents and Bar neuron subpopulations using channelrhodopsin-assisted circuit mapping (CRACM). In the second part we use optogenetics, *in vivo* fiber photometry, genetic ablation and Cre-mediated knockout, to define and contrast the roles of $Bar^{Crh/Vglut2}$ neurons with the greater population of Bar^{Vglut2} neurons.

Results

Afferents to Bar

To define the upstream circuitry that may regulate Bar and control micturition, we used Cre-conditional retrograde rabies tracing in *Crh-IRES-Cre* mice to identify synaptic afferents to $Bar^{Crh/Vglut2}$ neurons (Figure 1A). Major sources of afferents include the bed nucleus of the stria terminalis (BnST), lateral preoptic area (LPOA), medial preoptic area (MPOA), median preoptic nucleus (MnPO), insular cortex, lateral hypothalamic area (LHA), ventromedial hypothalamus (VMH), central nucleus of the amygdala (CeA) and, spanning its entire rostral-caudal axis, the lateral and ventrolateral divisions of the periaqueductal gray matter

(vlPAG) (data not shown). These afferent sites correspond largely to those identified by Hou [20] in mice and by Valentino and colleagues in rats [18].

Separately, we placed injections of a non-conditional retrograde tracer, cholera toxin-b (CTb), into Bar of *Vgat-IRES-Cre::L10-GFP* or *Vglut2-IRES-Cre::L10-GFP* mice to characterize the inhibitory or excitatory nature of neurons (i.e. presence of cellular markers for synaptic GABA (Vgat+) or glutamate (Vglut2+) release), that project to this brainstem region. Colocalization of GFP reporter for Vgat with CTb was observed in subsets of neurons in all rabies-eGFP labeled sites, with the exception of the rostral-midrostral level of PAG and the MnPO. Colocalization of GFP reporter for Vglut2, with CTb (Figure 1B,C) was observed predominantly in the LHA, VMH, MnPO, PAG and insular cortex, but not in the BnST, LPOA or CeA. These findings reveal that Bar may receive both inhibitory and excitatory inputs from a considerable number of upstream sites implicated in diverse behaviors that may or may not be related to micturition. We then used Cre-conditional anterograde tracing to confirm that axon terminals from retrogradely-identified afferent sites project directly to Bar. Figure 1C shows axons from LHA^{Vglut2} neurons to Bar that appear to project to the extensive dendritic arbor of $Bar^{Crh/Vglut2}$ neurons (underneath the 4^{th} ventricle and dorsal to Bar) and to the core of Bar. By contrast, axon terminals from PAG^{Vglut2} neurons terminate over the dorsal dendrites and even more densely in the core of Bar (Figure 1D).

Distribution of PAG→Bar and LHA→Bar projecting neurons

Given the well-established roles of both the PAG and the hypothalamus in affecting bladder pressure or controlling the bladder volume threshold for micturition [7, 14, 23, 26–28], we selected these two sites for further characterizing the identity and functional contribution of neurons that provide regulation of Bar in neural control of micturition behavior. We first sought to determine the anatomical location of excitatory neurons in the PAG projecting to Bar ($PAG^{Vglut2\ ->\ Bar}$) and found that these were spread across the rostral to caudal, lateral-ventrolateral extent of the PAG. We then asked whether Bar-projecting neurons in the LHA ($LHA^{Vglut2\ ->\ Bar}$) also contained orexin or melanin-concentrating hormone (two peptides that define prominent LHA populations). We did not see any retrogradely rabies-labeled (GFP+) neurons co-labeled with orexin or melanin-concentrating hormone.

Glutamatergic LHA and PAG neurons are functionally connected to Bar

We next tested for functional synaptic connectivity between glutamatergic LHA or PAG axons and postsynaptic Bar neurons, using channelrhodopsin-assisted circuit mapping (CRACM). To do so, we placed unilateral injections of AAV.ChR2.mCherry into the LHA or the PAG of *Crh-IRES-Cre* crossed to *L10-GFP* reporter mice. Photostimulation of channelrhodopsin-2 (ChR2)-expressing presynaptic terminals, in *ex vivo* slices containing Bar, evoked excitatory postsynaptic currents (EPSCs) with short latency that persisted following TTX/4-AP application (Figure 1E–J), demonstrating monosynaptic connectivity, and EPSCs were eliminated by the glutamate receptor antagonist DNQX. The GABA-A receptor antagonist bicuculline was bath-applied to block light-evoked inhibitory postsynaptic currents (IPSCs), so isolated EPSCs could be recorded.

We observed EPSCs in GFP+ and GFP− cells, suggesting broad connectivity to both $Bar^{Crh/Vglut2}$ neurons and to Bar^{Vglut2} neurons that may lack *Crh* expression. In PAG-injected cases, 80% of neurons exhibited monosynaptic connectivity, with light-evoked EPSCs in 28 of 35 GFP+ (i.e. putative $Bar^{Crh/Vglut2}$ cells) and in 20 of 25 GFP-negative (putative $Bar^{Crh\text{-}negative}$) neurons (Figure 1E,F, and S1A). In LHA-injected cases, more than 70% of cells exhibited monosynaptic connectivity, with light-evoked EPSCs recorded in 20 of 25 GFP+ and in 17 of 24 GFP− neurons (Figure 1H,I, and S1B). Importantly, since glutamatergic postsynaptic currents were detected in both GFP+ ($Bar^{Crh/Vglut2}$) and GFP− ($Bar^{Crh\text{-}negative}$) neurons, LHA and PAG axons projecting to Bar do not appear to target *Crh*-expressing neurons preferentially.

Activation of Bar-projecting glutamatergic PAG neurons induces detrusor activation and instant urinary incontinence

Given the functional, monosynaptic connectivity across the population of Bar neurons, we tested whether photoactivation of PAG^{Vglut2} terminals in Bar would be sufficient to trigger micturition. We placed unilateral injections of AAV.DIO.ChR2 into the PAG of *Vglut2-IRES-Cre* mice and implanted an optic fiber over Bar (Figure 2A–F). We then photostimulated ChR2-expressing terminals in Bar at a frequency of 10 Hz. Optogenetically activating PAG^{Vglut2} axon terminals produced void responses in 80% of trials when mice were awake and freely moving (Figure 2F) recorded with our noninvasive Micturition Video Thermography (MVT) void spot assay (Figure S2A). These voids were small in size (typically less than 100 μL) and immediate, with urine dropped at the exact position the mouse was at the moment when stimulation started. Cystometry (CMG) recordings under anesthesia revealed that 97% of $PAG^{Vglut2 \text{ -> } Bar}$ stimulations triggered an increase in bladder pressure, and 28 of 29 of those contractions resulted in a void (Figure 2D–F, and S2B,C).

Activating glutamatergic LHA axons in Bar induces bladder contractions and continent-appearing voiding behavior

Using an identical experimental design, we then optogenetically activated LHA^{Vglut2} axon terminals within Bar (Figure 2G–L) and found that this too increased detrusor activity and produced voiding in both awake and anesthetized mice (Figure 2J–L, and S2D). A typical voiding sequence consists of the mouse searching for, then moving to a ‘designated’ place, typically one of the cage corners. Micturition events evoked by stimulation of $LHA^{Vglut2 \text{ -> } Bar}$ axons occurred inconsistently and with a delay, but always after the mouse moved to the corner of the cage (Figure 3A,B). We also assessed changes in bladder pressure under anesthesia while optogenetically stimulating LHA^{Vglut2} terminals within Bar (Figure 3C). In this setting, 87% of stimulations evoked a change in bladder pressure, with a much higher likelihood to void if pre-stimulation pressure was elevated, indicating that whether the mice voided in response to stimulation depended on fullness of the bladder (Figure 3D). After a light-evoked voiding contraction, bladder pressure returned to baseline, albeit more slowly than what is normal after spontaneous bladder emptying (Figure 3C, S3C).

Though activation of these excitatory afferents reliably produced voiding, the response profile of stimulating axon terminals from the two afferent regions was distinct. In contrast

to voids that followed stimulation of $LHA^{Vglut2\ ->\ Bar}$ terminals, voiding evoked by photostimulation of $PAG^{Vglut2\ ->\ Bar}$ terminals did not resemble typical, continent voiding behavior in the awake condition. Furthermore, stimulation of LHA^{Vglut2} terminals in awake mice resulted in significantly fewer void responses than stimulation of PAG^{Vglut2} terminals within Bar. Axon terminals of excitatory neurons projecting from LHA and PAG are functionally connected to both glutamatergic $Bar^{Crh/Vglut2}$ and $Bar^{Crh\text{-}negative}$ neurons. This suggests that specific Bar neurons could be important for coordinating downstream bladder control.

Direct optogenetic stimulation of glutamatergic Bar neurons triggers micturition

To compare direct activation of Bar neurons with photoactivation of axon terminals from $PAG^{Vglut2\ ->\ Bar}$ and $LHA^{Vglut2\ ->\ Bar}$ terminals, we optogenetically stimulated Bar^{Vglut2} cell bodies (Figure 4A–E) at a frequency of 10 Hz (Bar neurons in *ex vivo* slices consistently respond with action potentials at this stimulation frequency; Figure S4A–C, [29]). Light-stimulation of Bar^{Vglut2} neurons in awake mice produced an immediate void response in 70% of trials (Figure 4E,J, and S3A). Similar to PAG^{Vglut2} axons in Bar, photostimulating Bar^{Vglut2} neurons resulted in incontinent behavior; mice did not go to a cage corner before voiding. If the mouse was walking, light stimulation produced loss of urinary continence mid-stride. While under anesthesia, photostimulation produced a large and sustained pressure change in 100% of trials, 91% of which also led to a void (Figure 4C–E,K, and S4D). Voiding responses were immediate, suggesting a direct effect on urethral sphincter activity, and bladder pressure remained elevated for the duration of the stimulus, after which it rapidly returned to baseline (Figure 4C,D, and S4D). The sustained effect of light stimulation on detrusor activity may be a consequence of the bladder collapsing onto the catheter with ongoing light-evoked bladder contractions.

Optogenetic activation of $Bar^{Crh/Vglut2}$ soma produces comparably modest voiding responses

We next stimulated $Bar^{Crh/Vglut2}$ neurons, which are roughly half of Bar neurons. These neurons are assumed to be critical for micturition [20], and in preliminary experiments chemogenetic activation of $Bar^{Crh/Vglut2}$ neurons increased void frequency in awake mice (Figure S4F,G) and increased baseline bladder pressure with lower amplitude contractions while under anesthesia (Figure S4H). Surprisingly, however, optogenetic activation of *Crh*+ ($Bar^{Crh/Vglut2}$) neuron somas (Figure 4F–I) drove voiding responses in only 5 of 82 stimulation trials (6%) in awake mice (Figure 4I). Furthermore, these voiding events were delayed (Figure 4J) compared to light stimulation of glutamatergic neurons and behaviorally normal in that mice went to the cage corner before voiding (Figure S3B). Detrusor activity recorded in anesthetized mice, revealed that stimulating $Bar^{Crh/Vglut2}$ neurons frequently increased bladder pressure, but voiding occurred in only 17% of trials (Figure 4G–I, and S4E).

While it is clear that photostimulation of $Bar^{Crh/Vglut2}$ neurons can influence bladder pressure, the magnitude and frequency of voiding responses was far less than that observed following photostimulation of the larger Bar^{Vglut2} population and of PAG^{Vglut2} and LHA^{Vglut2} terminals within Bar. Given that the voiding responses were delayed and detrusor

activity was not sustained following light stimulation of $Bar^{Crh/Vglut2}$ neurons as compared to activation of $PAG^{Vglut2 \rightarrow Bar}$ and $LHA^{Vglut2 \rightarrow Bar}$ terminals (Figure 4K, S3D,E), these findings directly challenge the primacy of $Bar^{Crh/Vglut2}$ neurons in initiating micturition behavior.

Selective ablation of Bar neuron subpopulations results in abnormal micturition behaviors

These *in vivo* optogenetic findings diverge sharply with previous claims regarding the role and importance of $Bar^{Crh/Vglut2}$ neurons in micturition behavior [20]. To further explore their role in bladder control, we tested the necessity of $Bar^{Crh/Vglut2}$ and Bar^{Vglut2} neurons for detrusor activation and micturition behavior. We placed bilateral injections of an AAV that expresses Cre-dependent Diphtheria Toxin subunit-A (AAV.mCherry.DIO.DTA, Figure 5A, S5A–D, [30]) into Bar of either *Vglut2-IRES-Cre, Crh-IRES-Cre* or *C57Bl6/J* control mice (Figure 5B–D). We then assessed micturition-related behaviors on post-operative days (POD) 5, 10, 15 and 20 in awake mice. DTA-mediated ablation of the larger population of Bar^{Vglut2} neurons, which includes $Bar^{Crh/Vglut2}$ neurons, resulted in urinary retention. This phenotype is similar to that observed following large, non-specific lesions of the PMC [5, 13, 14, 31]. During the 2-hour void spot assay at POD15, some mice did not void at all, while others released many, small, incontinent-appearing voids at random locations (Figure 5B,C, and S5E,F). The voids were characterized as overflow incontinence leaks (see method details), rather than continent or volitional voids because urine drops appeared while the mouse was walking and the mice did not exhibit evidence of continent voiding in a corner or alongside a wall. Ablation of Bar^{Vglut2} neurons and hence excitatory neurotransmission from this region resulted in moribund mice necessitating euthanasia in most mice by POD 20. CMG recordings in these mice were performed within 3 weeks of surgery, and confirmed urinary retention (Figure 5D upper panel, and S5G).

In sharp contrast to the severe urinary retention and leak-incontinence after ablation of Bar^{Vglut2} neurons, selective ablation of $Bar^{Crh/Vglut2}$ neurons with DTA, in *Crh-IRES-Cre* mice, resulted in only mildly abnormal micturition behaviors, ranging from increased urinary frequency to retention-like phenotypes (Figure 5A–D, S5E,F). In some mice a trend toward decreased void number could indicate retention and, consistent with this possibility, we found that when voids did occur they were larger in size. The behaviors associated with typical, awake mouse voiding remained unchanged; all awake mice with complete $Bar^{Crh/Vglut2}$ neuron ablation were still capable of voiding normally in a cage corner (Figure 5B,C), indicating that supraspinal control over bladder detrusor and sphincter muscle function remained intact. Under anesthesia, the fill-void cycle on CMG was delayed in DTA-ablated *Crh-IRES-Cre* mice (Figure 5D lower panel, and S5G), however, pre-voiding contractions occurred during the filling phase. Thus, the *Crh*-expressing subpopulation of Bar^{Vglut2} neurons can increase bladder pressure, but neither acutely stimulating nor eliminating them grossly alters normal, continent voiding behavior.

Deleting *Crh* from Bar neurons in adulthood, does not significantly affect voiding behavior

To determine whether CRH neuropeptide release by Bar neurons contributes to bladder control, as has been suggested by prior pharmacology experiments [32–34], we selectively disrupted the ability of $Bar^{Crh/Vglut2}$ neurons to express *Crh*, while leaving glutamatergic

neurotransmission intact. AAV.Cre injected bilaterally into Bar of homozygous floxed-*Crh* mice (*Crh*$^{fl/fl}$) [35] caused recombination of loxP sites surrounding exon 2 of the *Crh* gene, producing a functional knockout (KO) of *Crh* in transduced Bar neurons (Bar$^{Crh\text{-}KO}$) (Figure 6A). Control *Crh*$^{fl/fl}$ mice received bilateral injections of AAV.mCherry (Bar$^{Crh\text{-}control}$). After confirming that AAV.Cre injections produce complete deletion of exclusively *Crh*, using in-situ hybridization to detect *Crh* and *Vglut2* mRNA (Figure 6A lower panel, and S6A,B), we placed bilateral injections of AAV.Cre.mCherry into Bar and recorded the frequency of voiding and voided volumes in awake mice before surgery and in 10-day post-operative intervals for 50 days. Surprisingly, complete bilateral deletion of the neuropeptide gene had no effect on any of the recorded micturition behavior parameters in awake mice (Figure 6B). Under anesthesia, Bar$^{Crh\text{-}KO}$ and Bar$^{Crh\text{-}control}$ mice exhibited fill-void cycles that were similar in length, with normal void contractions (Figure 6C,D). This suggests that, while *Crh* is a convenient marker for Bar$^{Crh/VGlut2}$ neurons, its expression in these neurons does not serve an essential role under the conditions studied here.

Neural activity patterns differ between Bar neuron subpopulations

To test whether the spontaneous, *in vivo* activity of select Bar neuronal populations correlates with specific phases of spontaneously occurring micturition, we used GCaMP6-based fiber photometry to measure activity in Bar^{Vglut2} or Bar$^{Crh/Vglut2}$ neurons in awake, freely-behaving mice (Figure 7A–C), while bladder pressure was recorded simultaneously, and saline infused continuously. We confirmed that neural activity correlated with void events (Figure 7D). Increased activity of Bar^{Vglut2} neurons preceded the initial rise in bladder pressure and lasted for a total of 40 seconds (Figure 7E,G), well beyond the duration of typical detrusor activity with void contractions. In contrast, Bar$^{Crh/Vglut2}$ neuron activity increased concomitant with bladder pressure. The greatest activity was during the micturition event and elevated activity sustained for approximately 25 seconds (Figure 7F,H). The strong temporal association of Bar$^{Crh/Vglut2}$ activity with bladder pressure [20] supports a role for these neurons in sustaining detrusor contractions, but the fact that activity of overall Bar^{Vglut2} neurons precedes that of Bar$^{Crh/Vglut2}$ neurons and the rise in bladder pressure (Figure 7I,J), suggest that non-*Crh* Bar^{Vglut2} neurons initiate micturition, including bladder contractions. Bar^{Vglut2} neurons appear to function as an on-off switch for micturition, as their spontaneous activity precedes, then correlates with peaking detrusor activity, and activating these neurons immediately triggers voiding.

Discussion

Our results identify excitatory, subcortical inputs to Bar from the PAG and LHA, with surprising differences in the voiding behavior evoked by each. Further, we challenge recent claims regarding the role of Bar^{Crh} neurons by showing that neither *Crh* expression, nor the activity of these neurons is critical for voiding.

Glutamatergic LHA and PAG neurons are functionally connected to Bar neurons and these monosynaptic connections potently influence voiding behavior (Figures 1–3). Interestingly, the effects of *in vivo* optogenetic stimulation of these separate afferents produces divergent physiological responses. Activation of PAG axon terminals in Bar reduced the latency to

void, such that the animal did not search for, or did not reach, a designated void location. This immediate and potent void response to optogenetic stimulation is consistent with a role for the PAG in the micturition reflex pathway and provides a more detailed understanding of the cellular basis of this circuitry. Electrical stimulation within the PAG has been shown to evoke bladder contractions and micturition [36–39]. And pharmacological modulation of PAG circuitry alters the bladder volume threshold for micturition [24–26], suggesting that the PAG may upregulate the activity of Bar neurons that control micturition. Future studies exploring how subsets of neurons in the PAG provide synaptic gain control over Bar to allow voiding are eagerly awaited. In addition, it will be important to understand if known spinal afferents to the PAG can inhibit the micturition reflex and, if so, which PAG cell populations are postsynaptic targets of the spinal input.

Higher modulatory brain centers that are not directly implicated in the supraspinal micturition reflex pathway but feed into it, also play a role in facilitating bladder emptying. In contrast to the response when stimulating PAG terminals, stimulating LHA axon terminals in Bar, did not upset the typical sequence of micturition behavior; the animal had time to move to a designated void location prior to voiding. Also, in the awake condition, stimulating LHA^{Vglut2} terminals resulted in significantly fewer light-evoked voids than stimulating PAG^{Vglut2} terminals within Bar, and this effect disappeared under anesthesia. Divergent effects of these two afferents suggest that LHA terminals partially, but incompletely activate Bar^{Vglut} neurons, or that within Bar they more potently depolarize neurons that drive detrusor contractions than sphincter relaxation. We cannot rule out the possibility that back-propagating action potentials in $LHA^{Vglut2\ ->\ Bar}$ axons depolarize LHA neurons, whose collateral axons to other brain regions may promote or coordinate continent voiding behaviors. Whichever the mechanism, the impact of this hypothalamic afferent is likely related to adapting bladder control to environmental context or homeostatic needs.

It is important to keep in mind that cystometry involves saline infusion into the bladder, an intervention which speeds up the bladder fill-void cycle and hence increases the likelihood of stimulating a full bladder. In our study, LHA neurons responded to light stimulation more consistently when bladder pressure was elevated. This is in agreement with early studies using transections and suction lesions in cats, reporting that the posterior lateral hypothalamus plays a facilitory role in micturition and when lesioned a higher bladder pressure is needed before a voiding contraction is triggered [7, 40]. Bar-regulation by ‘extra-reflex’ afferents probably depends on a pressure-sensing (sacral spinal cord efferent) midbrain center to relay bladder fullness information [41], consistent with our finding that glutamatergic input from the PAG more more reliably triggers voiding.

Barrington’s nucleus in the mouse is under broad afferent control. While outside the scope of the current study, it is tempting to speculate that different pathways in the mouse subserve different behaviors; for example, micturition is differentially influenced by stress, maternal behavior, social dominance behaviors (such as territory marking), nociception, cardiovascular demands, fluid balance, hormone homeostasis, and sleep [42–44].

Recent studies have described a role for Bar neurons in regulating micturition behavior in male mice in response to olfactory cues, showing that these neurons are active with socially

relevant micturition behavior and that their inhibition decreases territorial marking behavior [20, 21, 45]. *Crh*-expressing neurons have long been used as a convenient proxy cellular marker for the anatomic Bar, and studies have used this cell population for the identification of circuit nodes providing afferent inputs to Bar. While injury to or inhibition of the region containing Bar prevents voiding and results in urinary retention [5–7, 11, 12, 31], we found that mice with complete bilateral genetic lesion of the $Bar^{Crh/Vglut2}$ neuron population still exhibited relatively normal voiding behaviors (Figure 5). These mice had longer fill-void cycles and voided larger volumes of urine, but did not display frank urinary retention. We did observe an increase in the baseline bladder pressure as well as a decrease in void contraction amplitude while chemogenetically activating $Bar^{Crh/Vglut2}$ neurons, which resulted in more frequent, smaller voids.

However, optogenetic stimulation of the $Bar^{Crh/Vglut2}$ cell population produced only modest, inconsistent responses, in sharp contrast to light stimulation of all Bar^{Vglut2} neurons, which yielded immediate, strong bladder contractions with voiding. Thus, *Crh*-expressing Bar neurons are neither necessary nor sufficient for voiding, although their activity contributes to bladder control by increasing detrusor tone (Figure 4 and 4SD–F). While *Crh* remains a useful marker for a subpopulation of Bar^{Vglut2} neurons that augment detrusor contraction, they represent only a portion of the neurons involved.

Additionally, selectively disrupting the ability of $Bar^{Crh/Vglut2}$ neurons to release CRH peptide while leaving glutamatergic neurotransmission intact, did not alter voiding frequency, voided volume, or micturition associated behaviors. Knockout of CRH did not appear to affect bladder capacity or voiding efficiency (Figure 6). The trend toward increased detrusor activity prior to voiding contraction in these mice suggests that expression of *Crh* in Bar^{Crh} neurons may function to suppress detrusor activity during the filling phase.

The concept that CRH release may function to inhibit the bladder from ‘unnecessary’ contractions or otherwise act as a ‘brake’ upon Bar in triggering voiding, is supported by studies using mouse models of social stress, which report retentive phenotypes in the setting of elevated CRH neuropeptide levels [46–48]. Furthermore, intrathecal administration of CRH in rats reduces the magnitude of bladder contractions following microinjection of glutamate into Bar, whereas the CRH receptor antagonist (D-PheCRHt2) has the opposite effect [32], providing further support for this hypothesis. Consequently, Bar^{Crh} neurons may be an appropriate therapeutic target for suppressing detrusor activity, as would be desired in the setting of an overactive bladder. Alternatively, Bar^{Crh} neurons and their release of CRH may be involved in other pelvic, autonomic functions like colonic motility, as suggested by recordings in rats [49, 50].

Our *in vivo* fiber photometry experiments demonstrate the existence of physiological heterogeneity among Bar neuron populations (Figure 7). We found that Bar^{Vglut2} neurons are active prior to voiding contractions and that their activity is phase-advanced relative to $Bar^{Crh/Vglut2}$ neurons and detrusor activity. Because $Bar^{Crh/Vglut2}$ neurons become active with pressure rise, and peak with void contraction toward the end of the voiding, these neurons likely augment bladder contraction. Furthermore, Keller and colleagues [21]

showed that Bar^{Esr1} neurons, similar to $Bar^{Crh/Vglut2}$ neurons, track bladder pressure changes. According to this study, Bar^{Esr1} neuron activity peaks when urine appears, which is approximately 3 seconds prior to the voiding contraction peak, and this likely corresponds with activity of the external urethral sphincter (EUS) and passing of urine. It remains unclear whether the summed activity of Bar^{Esr1} plus $Bar^{Crh/Vglut2}$ neurons accounts for our overall Bar^{Vglut2} photometry data, and we cannot exclude the possibility that our approach (recording bulk calcium signals from glutamatergic tegmental neurons in and around Bar) incorporates signals from glutamatergic neurons outside Bar, some of which exhibit spiking activity that increases or decreases in association with bladder filling and voiding [29].

Non-*Crh* glutamatergic Bar neurons with estrogen receptor expression (Bar^{Esr1}) project axons that preferentially target interneurons in the spinal cord, triggering bursts of EUS activity that allow voiding [21]. These recent findings complement our results, since they demonstrate both a necessary and sufficient role for Bar^{Vglut2}, but not $Bar^{Crh/Vglut2}$ neurons in initiating micturition, identifying *Esr1* as a marker for some or all of the non-*Crh*-expressing neurons in Bar, which are clearly important for micturition behavior.

Studies that distinguish subtypes of glutamatergic Bar neurons with a specific role in orchestrating different components of the total void sequence through separate afferent circuits, are greatly anticipated. Also, the extent to which CRH release in Bar affects EUS-controlling neurons – either at the level of Bar (affecting Bar^{Esr1} neuron activity) or of interneurons in the spinal cord – remains to be addressed [51, 52].

In conclusion, our results help elucidate the neural networks that control bladder function through Bar neurons. Taken together, and using a novel, non-invasive assay for micturition behavior in awake, freely-behaving mice, this study shows that neurons in brain regions upstream of Barrington's nucleus provide potent synaptic control over its neurons. In addition, distinct voiding-related behavior in response to different circuit-based stimulations indicates that specific nodes orchestrate different components of the total void sequence of behavior.

While a critical role for Bar in bladder control has long been appreciated, the specific Bar cell populations subserving this control, initiating micturition in particular, have remained unresolved or otherwise controversial. We show here for the first time that glutamatergic Bar neurons are both necessary and sufficient for micturition behavior. In addition, our findings with optogenetic stimulation and genetic ablation of $Bar^{Crh/Vglut2}$ neurons, *Crh* deletion, and *in vivo* monitoring of neural activity, suggest that $Bar^{Crh/Vglut2}$ neurons are not driving this behavior. Because neither *Crh* expression nor the neurons that express it are necessary for the overall population of Bar^{Vglut2} neurons to control bladder function, further studies examining the roles of non-*Crh*-expressing glutamatergic Bar neurons will likely identify subpopulations which play critical roles in the control of bladder function.

STAR Methods

LEAD CONTACT AND MATERIALS AVAILABILITY

All data and custom software are available upon reasonable request by contacting the corresponding author at aversteg@bidmc.harvard.edu

This study did not generate new unique reagents.

EXPERIMENTAL MODEL AND SUBJECT DETAILS

Mice—All animal care and experimental procedures were approved in advance by the National Institute of Health and Beth Israel Deaconess Medical Center Institutional Animal Care and Use Committee. Mice were housed at 21–23 °C with a 12-h light: 12-h dark cycle and ad libitum access to standard mouse chow (Teklad F6 Rodent Diet 8664) and water.

For all behavior studies and tracing studies, male mice between 6 and 20 weeks old were used. For electrophysiological studies male and female mice between 6 and 12 weeks old were used. Mice weighed between 20 and 30g. All Cre driver and lox reporter mice were used in the heterozygous state. *Crh fl/fl* mice were used in the homozygous state.

Mice used in this study were obtained from the Lowell or Jackson Laboratories and bred on a mixed background composed of primarily *C57Bl6/J.*

METHOD DETAILS

Viral injections and optical fiber implantation—Stereotaxic injections were performed as previously described [53]. In brief, mice were anesthetized with ketamine/xylazine (100/10 mg/kg i.p.), and placed into a stereotaxic apparatus (Kopf 940). After exposing the skull via a midline incision, a small burr hole was drilled for injection. A pulled-glass micropipette (~20 μm internal diameter) was lowered into the brain and AAV, CTb or modified rabies virus was injected by an air pressure system using picoliter air puffs through a solenoid valve (Clippard EV 24VDC) controlled by a Grass stimulator (model S48). The pipette was withdrawn 10 min after injection. The edges of the incision were re-apposed and secured in place with tissue adhesive (n-butyl cyanoacrylate, Vetbond). For post-operative care, mice were injected with meloxicam sustained release (4 mg/kg s.c.), before being placed on a heating pad where they were monitored until fully awake.

For chemogenetic experiments, mice received bilateral injections of AAV8.hSyn.DIO.hM3Dq.mCherry (University of North Carolina Vector Core). For electrophysiology (whole cell recordings) and *in vivo* optogenetic experiments, mice received unilateral injections with AAV9.CBA.Flex.rev.ChR2 (H134R).mCherry (University of Pennsylvania Vector core; Addgene #18916) or AAV8.DIO.mCherry (University of North Carolina Vector Core; #4981). For *in vivo* calcium imaging experiments, mice received unilateral injections of AAV1.hSyn.Flex.GCaMP6s (University of Pennsylvania Vector core). For electrophysiology/CRACM experiments, *Crh-IRES-Cre::L10-GFP* Cre-reporter mice to visualize $Bar^{Crh/Vglut2}$ neurons, received unilateral or bilateral injections with non-conditional AAV9.CAG.ChR2(H134R).mCherry (University of Pennsylvania Vector core; Addgene #20928). For neuron ablation experiments, mice received bilateral injections with

AAV10.EF1α.mCherry.DIO.DTA (P. Fuller, M. Lazerus; Beth Israel Deaconess Medical Center). For *Crh* knockout experiments, mice received bilateral injections with AAV8.hSyn.Cre.mCherry or AAV8.hSyn.mCherry (University of North Carolina Vector Core). For anterograde axonal tracing studies, mice received unilateral injections with AAV8.DIO.Syp.YFP (Virovek), AAV9.CBA.Flex.ChR2-mCherry, or AAV1.hSyn.Flex.GCaMP6s (University of Pennsylvania). For standard retrograde tracing, mice received unilateral injections with Cholera Toxin B Subunit (0.1% in PBS, Choleragenoid from Vibrio cholerae in Low Salt, List Biological laboratories; #104). For monosynaptic conditional retrograde tracing, the helper vectors AAV8.CAG.Flex.RG (Stanford Medicine, Gene Vector and Virus core) and AAV8.EF1α.Flex.TVA.mCherry (University of North Carolina Vector Core) were injected in a single surgery and pseudotyped G-deleted rabies; SAD.ΔG.EnvA.GFP (Salk Institute for Biological Studies, Viral Vector core) was injected 3–4 weeks later.

Using stereotaxic coordinates according to the Franklin and Paxinos mouse brain atlas [54], injections were targeted to Barrington's nucleus at coordinates from Bregma: AP; −5.40, DV; −3.70, ML; +/−0.68, into vlPAG at: AP; −4.20, DV; −2.70, ML; 0.35, or into LHA at: AP; −1.20, DV; −5.00, ML; 1.00. All injection volumes were between 10 and 60 nl in size. 4 to 6 weeks were allowed for protein production and transport into dendrites and axons before commencing experiments.

Optical fiber implantation.: Optical fibers were implanted during the same surgery as AAV injections. Fibers were made using Thorlabs fiber termination and polishing supplies, and quality tested. For optogenetics experiments, ceramic ferrules (FZI-LC-230, Kientec Systems) with optical fibers of 200 μm diameter core (FT200UMT, NA 0.39; Thorlabs) were implanted unilaterally over the PMC. For fiber photometry experiments, stainless steel ferrules (MM-FER2007-304-4500-P, Precision Fiber Products) with optical fibers of 400 μm diameter core (FT400UMT Multimode, NA 0.39; Thorlabs) were implanted unilaterally over the PMC. Fibers were affixed to the skull using dental acrylic.

Micturition Video Thermography (MVT) - non-invasive void spot assay (See also Figure S2).—We developed an assay to study mouse voiding behavior that combines the temporal resolution of a cystometrogram with the volume and spatial information of void spot analysis, as well as live recording of mouse behavior. Micturition Video Thermography (MVT; Figure S2A) is non-invasive and compatible with neuroscience techniques such as optogenetics, chemogenetics, and *in vivo* fiber photometry. In addition, it yields information about the timing of individual voids, separation of multiple voids in one location and for studying other behaviors.

Enclosures were assembled from laser-cut acrylic (#8560K211, McMaster-Carr) with taller walls that angle outward, allowing the view of inner cage corners at a low camera angle. Cages have no cage bottom and are open on top. A fresh, dry sheet of filter paper was placed underneath the acrylic enclosure immediately prior to each test (Cosmos F36-COSBLT12038, 360 gsm; Blick Art Supply). The paper absorbs urine from each void, allowing an estimate of voided volume from the area of diffusion as in previous reports [55, 56]. One chow pellet was placed on the cage floor to occupy the mouse during the 2-hour

recording. Water was withheld during recordings to eliminate confounds in bladder filling and voiding from inter-individual differences in water intake during the test and because bottle spillage obfuscates void spot analysis.

Pilot tests revealed wide variance in voiding behavior, with some mice not voiding for up to four hours and we tested a variety of methods to standardize bladder filling and voiding in a 2-hour test session. For all MVT experiments described in this study, mice were 'volume-loaded' prior to recordings by injecting 1 ml prewarmed 5% dextrose (s.c.). Mice were returned to their home cages briefly prior to being introduced to the experimental arena in order to prevent fluid drips (from the volume loading injection) or small stress-triggered voids, from contaminating the assay. After 5–10 minutes each mouse was placed on the filter paper in the enclosure and data was collected for two hours. Experiments were run always at the same time of day; during the late phase of the light cycle and into the dark cycle.

Thermal imaging.: We used an A65 camera (640 × 512 sensor array, FLIR), with a fixed 13 mm lens (45° × 37°) and a microbolometer sensor array that captures thermal radiation in the long-wave range (7.5–13 μm) at frame rates of ~7.5Hz.

A weighted base was positioned on a shelf above the array of test cages, the gooseneck adjusted and facing straight down, centered above the inner cage corners. To provide optimal thermal contrast for identifying the border between the convective cooling of void spots relative to the dry filter paper, the lower display limit was set to 2°C below the ambient thermal emission of dry filter paper on the cage floor and the upper limit was set at 38°C, which is slightly higher than the core body temperature and thermal emission of mice and voided urine, with a linear scale and a rainbow color palette. For in vivo calcium imaging experiments we used a FLIR C2 camera, as described in the 'in vivo fiber photometry' section below. All MVT recordings were 2 hours in duration with the exception of neuron ablation experiments in which runs were extended to 4 hours to be able to detect possible delays in voiding, or retention.

Void spot calibration, data analysis and presentation.: For determining volume from the area of 'thermal void spots', we generated calibration curves for warmed urine. Obtained pixel area was converted to cm^2 (y) and plotted against the initial fluid volume ejected from the pipettor (x). Using the inverse slope of the linear best-fit equations for these calibration tests, the urine volume was estimated.

In ResearchIR software, thermal seq files were converted to wmv video format with time-stamps. Manual review allowed identification of the time of voiding, defined as the first frame with a void hotspot appearing. A screenshot was captured for measuring the area once the spot had reached a stable maximum area and had stopped spreading, which was generally 10–15 minutes later. Using ImageJ (NIH), the screenshot image was converted to 8-bit grayscale, and thresholded. To convert pixel area to cm^2, for each recording the pixel area of a 10 cm^2 reflecting cardboard template was measured. This area constant, unique to every recording due to slight differences in camera height or angle, allowed for estimating voided volume using data from the volume/area calibrations described above.

‘Typical mouse voiding behavior’.: A typical voiding sequence of behaviors begins with the mouse leaving its ‘home’ corner where it spends most of the test session. It explores, rears, paces and or grooms for seconds, then walks to a corner or wall, turns around facing away from the corner, lifts up the tail and sits still for several seconds, the mouse then walks away from the hotspot of fresh urine that has appeared on the filter paper. Control mice exhibit these behavioral features in virtually all voids, and any voids lacking these features in our experimental mice (for example when a small amount of urine leaks mid-stride, in the cage center, or while the mouse is engaged in other behaviors) were categorized as incontinent leaks. Furthermore, voids smaller in size than 20 μl, usually consisting of multiple ‘drops in a streak’, were categorized as incontinent leaks. Possible volitional scent or novelty markings that occurred within the first minutes of the 2-hour recording and that did not exhibit the typical continent features, were excluded from analysis.

Cystometrograms (CMG)—Bladder catheter implantation was performed as described previously [57]. In brief, under inhaled isoflurane anesthesia, a midline abdominal incision was made to expose the urinary bladder and a flared PE-50 tubing was inserted in the bladder dome. The catheter was secured with purse-string sutures (6–0 Polypropylene, Syneture) and the incision site was sutured closed around the tubing. For anesthetized CMG measurements, urethane was injected i.p. (1.2 g/kg in sterile saline) at the end of the surgery. After 30 mins the catheter was connected to a pressure transducer (Transbridge TBM-4M) coupled to a computerized recording system (AD instruments, Labchart), and the signal was recorded at 10 kHz while saline was infused at a rate of 25 μl/min. Bladder pressure was recorded for approximately ninety minutes.

Conscious cystometrogram.: Catheters were surgically implanted into the bladder as described above for anesthetized cystometry, but without urethane injection. A sterile Fr3-french catheter (C30PU-RJV1307, Instech Labs, PA) was implanted into the bladder, the free end was tunneled subcutaneously and exteriorized in the neck region through a small incision and connected to a mouse vascular access harness with a capped pin port (VAH62AB, Instech labs, PA). Animals were allowed to recover for 5 days and given Sustained Release (SR) Meloxicam (4 mg/kg, s.c.) in a single dose at surgery, and enrofloxacin (2.27%, 5 mg/kg, s.c.) at surgery and for two subsequent days after surgery. Awake cystometry recordings were performed in a metabolic cage without the attachments for urine or feces collection, with filter paper flooring. The pin port of the harness was connected to a pump for saline infusion and a pressure transducer for bladder pressure recordings.

CMG voiding physiology and quantification.: In general, a voiding contraction starts with a steep rise in pressure, which slows, then peaks and declines once voiding begins. The void duration is 3–7 seconds, after which it takes ~10 seconds for the pressure to return to baseline.

Chemogenetic experiments and analysis—Thermography recordings of chemogenetic activation experiments were performed by injecting either saline (vehicle) or Clozapine-N-Oxide (CNO; 1 mg/kg i.p.) 10 minutes prior to commencement of MVT

recordings. Mice were monitored for two subsequent hours. Each mouse underwent this paradigm 2 times for vehicle and 2 times for CNO, and their behavioral responses in these runs were averaged.

Cystometry recordings under anesthesia with chemogenetic activation, were performed by first injecting saline, followed by Clozapine-N-Oxide (CNO; 1 mg/kg i.p.) after approximately 40 minutes, during the CMG recording.

Optogenetic experiments and analysis—For optogenetic experiments, a 473 nm LED (PlexBright Table-Top LED modules, Plexon) was modulated by an Arduino board, and Arduino Software (Arduino cc, Sketch) was used to set the rate and pulse duration of a TTL signal on pin 13. For stimulation protocols, the LED was modulated at 10 Hz for 30 or 60 seconds at a time with 5 ms pulse duration. Patch cables (MFP_240/250/2000–0.63_1m_FC-ZF1.25, Mono Fiberoptic Patchcord, Doric) were connected to the fiber implant through a zirconia mating sleeve (SZI-LC-SP, Kientec Systems). Laser power was set between 5 and 8 mW as measured at the tip of the optic fiber using a Thorlabs light meter. We estimate the light power delivered to the PMC region to be 250–400 mW/mm^2 (Deisseroth lab, brain tissue light transmission calculator). During thermography recordings, mice were monitored for two hours and in that time approximately 12 stimulations were given.

Littermate control mice had received a non-light excitable reporter; AAV.DIO.mCherry. Each mouse underwent this paradigm over three separate sessions spaced at least 2 days apart and their behavioral responses in these runs were averaged.

Cystometry recordings under anesthesia with optogenetic stimulation, were performed with the same stimulation protocol and light intensity as above. To analyze detrusor activity responses to photostimulation, we calculated the pressure increase ΔP ($P_{(t)} - P_{min}$; where P_{min} is the minimum value of the entire normalized pressure trace). A pressure change was considered a response if the cumulative pressure increase from baseline P_0 was > 5% within the first 10 seconds of stimulation (a best fit was applied from −60s to start of stimulation to obtain P_0).

In vivo* fiber photometry, conscious cystometrograms and analysis—In vivo* fiber photometry was conducted as previously described [58]. Using the Doric Lenses 1-site, 2-color Fiber Photometry system (FPS_1S2C_405/GFP_400–0.48), calcium-dependent GCaMP6s fluorescence was excited by 465 nm light and modulated at 515 Hz. To control for artifactual fluorescence arising due to motion or tissue movement, in later experiments we also recorded 405 nm light, modulated at 211 Hz. Both light streams were coupled through a Doric FMC5 mini cube. The emission light was collected by the same fiber, passed through the GFP filter in the mini cube and focused onto a photodetector (model 2151 femtowatt photoreceiver; Newport). The signal from the photoreceiver was recorded at 10 kHz using Labchart software (AD instruments). The signal was demodulated and downsized to 0.1s precision, then analyzed using custom Matlab scripts from Doric. Cystometry pressure and GCaMP recordings were always started and recorded simultaneously in separate channels (at 10 kHz) using Labchart software.

We let the AAV express for at least six weeks prior to the experiment. Five days post bladder catheter implantation, mice were connected to the optical patchcord and the pin port of the harness was connected to a pump for saline infusion. Intensity of light (465 nm) at the end of the patchcord was 0.1–0.2 mW. Mice that did not show significant baseline calcium transient were assumed to be technical failures and were excluded from further experiments. All photometry studies were conducted in a metabolic cage, with filter paper flooring and a thermal camera (FLIR C2) placed below the cage (cages are described in 'conscious cytometry section' of methods) and the video recording start-time was marked as a comment on the CMG recording. The FLIR camera recorded voids as heat signature on the filter paper and this was used for confirmation of the micturition events. Each photometry-awake CMG session included at least 7 events and mice were run 2–5 times over multiple days. All trials across all days were pooled to calculate the mean fluorescence changes, 60 seconds before and 60 seconds after micturition events, for each mouse.

Analysis.: Relative change in fluorescence was calculated as $\Delta F\ (F_{(t)}\text{-}F_0)/F_0$, where a best fit was applied to the entire trace to obtain fitted signal F_0. The 405 nm (isosbestic point) excited GCaMP fluorescence ($\Delta F/F_0^{(405)}$) was subtracted from the 465 nm excited calcium-dependent GCaMP fluorescence ($\Delta F/F_0^{(465)}$). Heatmaps and graphs were generated using custom Matlab scripts. $\Delta F/F_0$ was converted to a z-score for each event. In the fluorescence to pressure ratio graphs, the normalized $\Delta F/F_0$ was divided over the normalized bladder pressure, averaged per mouse. In general, all void contraction events were included if the cystometry trace showed a single contraction peak. In initial experiments, GCaMP6s fluorescence signal was not modulated and background fluorescence not subtracted. However, because the later experiments clearly distinguished calcium-dependent fluorescence signal from artefactual fluorescence that were due to motion or tissue movements, we choose in this study to include trials that do not have background signal subtracted, along with subsequent trials that do.

Max differential (dP/dt).: The max differential (dP/dt) was calculated for each event, and the max value preceding a void contraction (confirmed by thermal video), was considered to represent highest detrusor activity and our 0-line in the graphs.

The 'zero-lag' graph shows the GCaMP signal 60 seconds before and 60 seconds after the dashed 0-line (moment of highest detrusor activity). The 'random-lag' graph includes randomly selected (MATLAB randomizer function 'Randy') of 120 seconds of GCaMP trace for a similar number and for the same traces as in 'zero-lag'.

Electrophysiology—Brain slices were prepared as previously described [59] and after identifying GFP-expressing neurons in Bar, whole-cell recordings were performed as described previously [59]. To test functional synaptic connectivity of afferents from PAG or LHA with Bar neurons (PAG → Bar and LHA → Bar), we used channelrhodopsin-assisted circuit mapping (CRACM) to photostimulate ChR2-expressing axon terminals in the slice and recorded from cells that were GFP+ (putatively $Bar^{Crh/Vglut2}$) or GFP− (putatively *Crh*-negative Bar neurons). For photostimulation we used full-field 10 ms flashes of light (~ 10 mW/mm^2, 1 mm beam width, delivered at 0.1 Hz for a minimum of 30 trials), from a 5 W

LUXEON blue light-emitting diode (470 nm wavelength; # M470L2-C4; Thorlabs, Newton, NJ, USA) coupled to the epifluorescence pathway of the microscope.

Brain blocks containing the injection sites and recorded brain slices, were placed overnight in 10% buffered formalin before sectioning for histology as described below. We confirmed the location of the ChR2-mCherry expressing neurons in the PAG and LHA injection sites as well as ChR2-positive terminals from these afferent neurons to Bar.

Voltage clamp and current clamp mode recordings were performed in ACSF using a K-gluconate-based pipette solution [59]. To record photo-evoked EPSCs, 5 mM QX314 was added to the pipette solution, 1 mM bicuculline to the ACSF, and recordings were conducted at V_h = −60 mV. To test monosynaptic connectivity, photo-evoked EPSCs were recorded in the presence of the voltage-gated sodium channel blocker tetrodotoxin (TTX; 1 μM) and potassium blocker 4-AP (1 mM). Photo-evoked EPSCs that persist in the presence of TTX/4-AP are considered to be evoked by monosynaptic connectivity [60, 61].

Recordings in current-clamp mode were performed to determine *in vitro* how Bar neuronal firing is entrained by different photostimulation frequencies. Recordings were conducted in Bar neurons from *Crh-IRES-Cre* or *Vglut2-IRES-Cre* mice that had received injections of AAV.DIO.ChR2 in Bar. We recorded in current-clamp mode at resting membrane potential (−50 mV ± 5 mV; n = 29 neurons) and photostimulated the recorded neurons using trains of light pulses (pulse duration; 5 ms, train frequency; 0.5 Hz, 1 Hz, 2 Hz, 5 Hz, 10 Hz, 20 Hz and 40 Hz, and train duration; 60 s). We confirmed the location of ChR2-mCherry expressing somata, as well as biocytin-filled recorded-from neurons, posthoc, in the PMC region.

Analysis.: Data was analyzed using Clampfit 10 (Molecular Devices), Mini Analysis 6 software (Synaptosoft), and MATLAB (MathWorks). The latency of photo-evoked EPSCs was calculated as the time difference between the onset of light stimulation and onset of the EPSC. The charge of the photo-evoked EPSCs was calculated as area under the curve of the evoked synaptic event. Action potential firing of Bar neurons expressing ChR2 in response to trains of light pulses was analyzed using MATLAB. Only action potentials that reached or passed 0 mV were counted. For examining differences in the distribution of sEPSC amplitudes, MATLAB was used to generate normalized frequency distributions and these were compared using a Kolmogorov-Smirnov test followed by unpaired t-tests.

Ablation experiments and analysis—For DTA-mediated ablation experiments, thermography recorded behavior trials were run at 4 different times post-surgery: post-operative day (POD) 5, 10, 15 and 20.

Cystometry recordings for neuron ablation experiments in *C57Bl6/J* and *Crh-IRES-Cre* mice were performed after the POD 20 awake behavior recording. In *Vglut2-IRES-Cre* mice, CMG recordings were performed within 3 weeks following surgery since these mice became moribund at around POD 20.

Brain sections including the core of Bar, and adjacent brain sections on either side, were histologically analyzed. We confirmed absence of GFP+ ($Bar^{Crh/Vglut2}$ or Bar^{Vglut2}) neurons

in the injection site; only complete bilateral hits with no green neurons remaining in the Bar region were included for analysis.

Cre-mediated KO of Crh and analysis—We recorded thermography/awake behavior every ten days for 50 days, to capture the timepoint at which mRNA and peptide for Crh had become completely absent from the Cre-recombined neurons in the injection site.

Cystometry recordings for *Crh* knockout experiments were performed after the time-course thermography trials, at POD 55–65.

Littermate control mice received bilateral injections with a reporter vector; AAV.mCherry and were tested and analyzed as Crh-KO. For analysis of 'non-voiding contractions' parameter, pressure changes larger than 10% of the 'average void contraction amplitude' were counted. We confirmed that there was no *Crh* mRNA remaining in Bar after bilateral AAV.Cre injection. Only complete bilateral hits were included for analysis.

Perfusion/histology/ISH—At the end of the experiment, mice were terminally anesthetized with 7% chloral hydrate, and transcardially perfused. Brains and in some cases spinal cords were removed for further analysis, then cut into 30 or 40 μm thick tissue sections on a freezing microtome (Leica model X-2000) for identification of AAV injection site and approximate fiber tip location.

Immunohistochemistry was performed as described previously [53]. All antisera used in this study are listed in the KRT table. Mice with missed injections, incomplete hits, or incorrect fiber placement were excluded from analysis.

RNAscope.: *In situ* hybridization was performed according to the Advanced Cell Diagnostics (ACD) manual multiplex fluorescent protocol, with an extra wash at all washing steps. We used Mm-Crh-C2 and -C1 probes for mouse corticotropin releasing hormone (ACD #316091-C2 and -C1) and Mm-Slc17a6-C3 for vesicular glutamate transporter 2 (ACD # 319171-C3).

Imaging and figures—Whole-slide fluorescence imaging was performed using a VS120 scanning microscope and VS-ASW software (Olympus). We used OlyVIA software (Olympus) to screen cases and identify the region containing transduced somata in Bar, PAG or LHA, or axonal projections to Bar. For heatmaps of LHA or PAG injection sites in our optogenetic *in vivo* cases, we outlined the region containing red ChR2-mCherry neurons atop an atlas template drawing [54] in Photoshop (Adobe). Injection sites were weighted according to each mouse' behavioral response (percentage light-evoked voids) and compiled in a color map using a Python script [62]. The region with deep-red color represents the maximum number of overlapping injection sites and maximum behavior response, with hues to orange and beige indicating less overlap.

QUANTIFICATION AND STATISTICAL ANALYSIS

Data analysis and statistics—Statistical analyses were performed using Prism 7 GraphPad software (San Diego, CA, USA) and are described in the respective figure legends

(including the statistical tests used, exact value of n, what n represents and dispersion and precision measures). No statistical method was used to predetermine sample sizes and statistical significance was defined as $p < 0.05$. (* < 0.05, ** < 0.01, *** <0.001, ****<0.0001). For randomization strategies MATLAB randomizer function 'Randy' was used. The investigators scoring the behavioral recordings were blinded to the recording conditions. All data presented met the assumptions of the statistical test employed. Experimental animals were excluded if histological validation revealed poor or absent reporter expression and this was established prior to data processing. n values reflect the final number of validated animals per group.

The chemogenetics experiments used 6 *Crh-IRES-Cre* mice [63]. The optogenetics experiments used 12 *Crh-IRES-Cre* mice, 9 *Vglut2-IRES-Cre* mice (Jax strain 028863 [64]) for soma stimulation, plus 4 respective controls for each, and 17 *Vglut2-IRES-Cre* mice for axon terminal stimulation. The photometry experiments used 4 *Crh-IRES-Cre* and 4 *Vglut2-IRES-Cre* mice. Whole cell recordings used 2 *Crh-IRES-Cre* and 5 *Vglut2-IRES-Cre* mice, and ChR2-assisted-circuit-mapping recordings used 19 males and females *Crh-IRES-Cre* crossed to *R26-loxSTOPlox-L10-GFP* reporter mice [63]. The neuron ablation experiments used 7 *Crh-IRES-Cre*, 4 *Vglut2-IRES-Cre* and 9 *C57Bl6/J* mice. The Crh knockout experiments used 15 floxed Crh mice (*Crh fl/fl*; Jax strain 002783 [35]), of which 7 for $Bar^{Crh\text{-}KO}$ and 8 as respective control. The tracing studies used *Crh-IRES-Cre, Vglut2-IRES-Cre* mice some of which crossed with *R26-loxSTOPlox-L10-GFP* reporter mice.

DATA AND CODE AVAILABILITY

The datasets and custom codes supporting the current study have not been deposited in a public repository but are available from the corresponding author on reasonable request.

Supplementary Material

Refer to Web version on PubMed Central for supplementary material.

ACKNOWLEDGMENTS

We thank Brad Lowell for generous use of shared mouse lines and equipment, David Olsen (*Crh-IRES-Cre* mice and *R26-loxSTOPlox-L10-GFP* reporter mice) and Joseph Mazjoub (Crh^{flox} mice). We thank Luca Szczpanik for help with data analysis, Lian Guo for help with cystometry, Arjan Gijsberts (IIT, Genova IT) for custom Matlab scripts and codes, Michael Lazerus and Patrick Fuller (BIDMC, Boston USA) for generating the AAV-DIO-DTA construct and vector, Pavlos Gorelik (HMS-instrumentation core facility, Boston USA) for help with generating behavior cages. We especially acknowledge Patrick Fuller for his advice and constructive criticism of early versions of this manuscript, Brad Lowell and Clif Saper, and members of the laboratories for general support, helpful discussions and comments on the manuscript. This work was supported by the NIH (grant P20DK103086 MLZ and RO1 DK113030 MLZ).

References

1. Barrington FJ, The relation of the hind-brain to micturition. Brain, 1921 44: p. 23–53.
2. Koyama Y, Ozakiand H, and Kuru M, Interference between detrusor nucleus and the pontine urine-storage an electromyographical external urethral nucleus. The Japanese Journal of Physiology, 1966 16: p. 291–303. [PubMed: 5297695]
3. Kuru M and Yamamoto H, Fiber Connections of the Pontine Detrusor Nucleus (Barrington). The Journal of Comparative Neurology 1964 123: p. 161–186. [PubMed: 14219662]

4. Rampal G and Mignard P, Behaviour of the Urethral Striated Sphincter and of the Bladder in the Chronic Spinal Cat. Pfliigers Arch, by Springer-Verlag 1975, 1975 353: p. 33–42.
5. Barrington FJ, The effect of lesions of the hind- and mid-brain on micturition in the cat. Quarterly Journal of Experimental Physiology, 1925 15: p. 81–102.
6. Barrington FJ, Affections of micturition resulting from lesions of the nervous system. Proceedings of the Royal Society of Medicine, 1927 20: p. 722–727.
7. Tang PC and Ruch TC, Localization of brainstem and diencephalic areas controlling the micturition reflex. The Journal of Comparative Neurology, 1956 106(1): p. 213–45. [PubMed: 13398495]
8. DeGroat WC, Nervous control of the urinary bladder of the cat. Brain Research, 1975 87: p. 201–211. [PubMed: 1125771]
9. Holstege G, et al., Anatomical and Physiological Observations on Supraspinal Control of Bladder and Urethral Sphincter Muscles in the Cat. The Journal of Comparative Neurology 1986 250: p. 449–461. [PubMed: 3760249]
10. Satoh K, et al., Localization of the micturition reflex center at dorsolateral pontine tegmentum of the rat. Neuroscience Letter, 1978 8: p. 27–33.
11. Fowler CJ, Neurological disorders of micturition and their treatment. Brain, 1999 122: p. 1213–1231. [PubMed: 10388789]
12. Sakibara R, Lower urinary tract dysfunction in patients with brain lesions. Handbook of Clinical Neurology, Autonomic Nervous System, Neurology of Sexual and Bladder Disorders, 2015 130(Chapter 15).
13. Komiyama A, Kubota A, and Hidai H, Urinary retention associated with a unilateral lesion in the dorsolateral tegmentum of the rostral pons. Journal of Neurology, Neurosurgery, and Psychiatry, 1998 65: p. 953–954.
14. Mallory BS, Roppolo JR, and De Groat WC, Pharmacological modulation of the pontine micturition center. Brain Research, 1991 546: p. 310–320. [PubMed: 1676929]
15. Sugaya K, et al., Electrical and chemical stimulations of the pontine micturition center. Neuroscience Letters, 1987 80: p. 197–201. [PubMed: 3683977]
16. Blok BFM, Willemsen ATM, and Holstege G, A PET study on brain control of micturition in humans. Brain, 1997 120: p. 111–121. [PubMed: 9055802]
17. Imaki T, et al., Differential Regulation of Corticotropin-Releasing Factor mRNA in Rat Brain Regions by Glucocorticoids and Stress. The Journal of Neuroscience, 1991 11(3): p. 585–599. [PubMed: 2002354]
18. Valentino RJ, et al., Evidence for widespread afferents to barrington's nucleus, a brainstem region rich in corticotropin-releasing hormone neurons. Neuroscience, 1994 62(1): p. 125–143. [PubMed: 7816195]
19. Vincent SR and Satoh K, CRF ir in the dorsolateral pontine tegementum- further studies on the micturition reflex system. Brain Research, 1984 308: p. 387–391. [PubMed: 6383518]
20. Hou XH, et al., Central Control Circuit for Context-Dependent Micturition. 2016 167(1): p. 73–86.
21. Keller JA, et al., Voluntary urination control by brainstem neurons that relax the urethral sphincter. Nat Neurosci, 2018 21(9): p. 1229–1238. [PubMed: 30104734]
22. VanderHorst VGJM, Gustafsson J-A, and Ulfhake B, Estrogen Receptor-' and -' Immunoreactive Neurons in the Brainstem and Spinal Cord of Male and Female Mice: Relationships to Monoaminergic, Cholinergic, and Spinal Projection Systems. The Journal of Comparative Neurology, 2005 488: p. 152–179. [PubMed: 15924341]
23. Tang PC, Levels of brain stem and diencephalon controlling micturition reflex. J Neurophysiol, 1955 18(6): p. 583–595. [PubMed: 13272043]
24. Kruse MN, et al., Pontine control of the urinary bladder and external urethral sphincter in the rat. Brain Research, 1990 532: p. 182–190. [PubMed: 2282512]
25. Matsumoto S, et al., Activation of mu opioid receptors in the ventrolateral periaqueductal gray inhibits reflex micturition in anesthetized rats. Neuroscience Letters, 2004 363: p. 116–119. [PubMed: 15172097]
26. Stone E, et al., GABAergic control of micturition within the periaqueductal grey matter of the male rat. J Physiol, 2011(589): p. 2065–2078. [PubMed: 21486804]

27. Noto H, et al., Electrophysiological analysis of the ascending and descending components of the micturition reflex pathway in the rat. Brain Research, 1991 549: p. 95–105. [PubMed: 1893257]
28. Andrew J and Nathan PW, The cerebral control of micturition. Proceedings of the Royal Society of Medicine, 1965 58: p. 553–555. [PubMed: 19994438]
29. Tanaka Y, et al., Firing of micturition center neurons in the rat mesopontine tegmentum during urinary bladder contraction. Brain Research, 2003 965: p. 146–154. [PubMed: 12591131]
30. Anaclet C, et al., Genetic Activation, Inactivation, and Deletion Reveal a Limited And Nuanced Role for Somatostatin-Containing Basal Forebrain Neurons in Behavioral State. The Journal of Neuroscience, 2018 38(22): p. 5168–5181. [PubMed: 29735555]
31. Satoh K, et al., Descending projection of the nucleus tegmentalis laterodorsalis to the spinal cord: studied by the horseradisch peroxidase method following hydroxy-dopa adminstration. Neuroscience Letters, 1978 8: p. 9–15. [PubMed: 19605141]
32. Pavcovich LA and Valentino RJ, Central regulation of micturition in the rat by corticotropin-releasing hormone from Barrington's nucleus. Neuroscience Letters, 1995 196: p. 185–188. [PubMed: 7501279]
33. McFadden K, et al., Overexpression of corticotropin-releasing factor in Barring- ton's nucleus neurons by adeno-associated viral transduction: Effects on bladder function and behavior. The European journal of Neuroscience, 2012 36: p. 3356–3364. [PubMed: 22882375]
34. Kiddoo DA, et al., Impact of state of arousal and stress neuropeptides on urodynamic function in freely moving rats. Am J Physiol Regul Integr Comp Physiol, 2006 290: p. R1697–1706. [PubMed: 16439667]
35. Zhang R, et al., Loss of hypothalamic corticotropin-releasing hormone markedly reduces anxiety behaviors in mice. Mol Psychiatry, 2017 22(5): p. 733–744. [PubMed: 27595593]
36. Noto H, et al., Excitatory and inhibitory influences on bladder activity elicited by electrical stimulation in the pontine micturition center in the rat. Brain Research, 1989 492: p. 99–115. [PubMed: 2752312]
37. Matsuura S, Downie JW, and Allen GV, Micturition evoked by glutamate micrinjection in the ventrolateral periaqueductal gray is mediated through barrington's nuclues in the rat. Neuroscience, 2000 101(4): p. 1053–1061. [PubMed: 11113354]
38. Taniguchi N, et al., A study of micturition inducing sites int he Periaqueductal gray of the mesencephalon. The journal of urology, 2002 168: p. 1626–1631. [PubMed: 12352469]
39. Skultety FM, Relation to periaqueductal gray matter to stomach and bladder motility. Neurology, 1959 9(3): p. 190–8. [PubMed: 13632880]
40. Tang PC, Levels of brain stem and diencephalon controlling micturition reflex. J Physiol, 1955 18(6): p. 583–95.
41. Athwal BS, et al., Brain responses to changes in bladder volume and urge to void in healthy men. Brain, 2001 124: p. 369–377. [PubMed: 11157564]
42. VanderHorst VGJM, Terasawa E, and Ralston HJ, Estrogen receptor immunoreactive neurons in the brainstem and spinal cord of the female rhesus monkey: species-specific characteristics. Neuroscience, 2009 158: p. 798–810. [PubMed: 18996446]
43. Kuipers R and Holstege G, Afferent Projections to the Pontine Micturition Center in the Cat. The Journal of Comparative Neurology 2006 494: p. 36–53. [PubMed: 16304684]
44. Sutcliffe JG and DeLecea L, The Hypocretins: Excitatory Neuromodulatory Peptides for Multiple Homeostatic Systems, Including Sleep and Feeding. Journal of Neuroscience Research, 2000 62: p. 161–168. [PubMed: 11020209]
45. Yao J, et al., A corticopontine circuit for initiation of urination. Nat Neurosci, 2018 21: p. 1541–1550. [PubMed: 30361547]
46. Butler S, et al., Murine social stress results in long lasting voiding dysfunction. Physiology & Behavior, 2018 183: p. 10–17. [PubMed: 28988966]
47. Wood SK, et al., Social stress-induced bladder dysfunction: potential role of corticotropin-releasing factor. Am J Physiol Regul Integr Comp Physiol, 2009 296: p. R1671–1678. [PubMed: 19279290]
48. Chang A, et al., Social stress in mice induces voiding dysfunction and bladder wall remodeling. Am J Physiol Renal Physiol, 2009 297: p. 1101–1108.

49. Holstege G, How the Emotional Motor System Controls the Pelvic Organs. Sexual Medicine Reviews, 2016 4: p. 303–328. [PubMed: 27872027]
50. Rouzade-Dominguez M-L, et al., Convergent responses of Barrington's nucleus neurons to pelvic visceral stimuli in the rat: a juxtacellular labelling study. European Journal of Neuroscience, 2003 18: p. 3325±3334. [PubMed: 14686905]
51. Holstege G, et al., Anatomical and Physiological Observations on Supraspinal Control of Bladder and Urethral Sphincter Muscles in the Cat. the journal of comparative neurology, 1986 250: p. 449–461. [PubMed: 3760249]
52. Holstege G, Kuypers HGJM, and Boer RC, Anatomical evidence for direct brain stem projections to the somatic moto-neuronal cell groups and autonomic preganglionic cell groups in cat spinal cord. Brain Research, 1969 171: p. 329–333.
53. Verstegen AMJ, et al., Barrington's nucleus: Neuroanatomic landscape of the mouse "pontine micturition center". The Journal of Comparative Neurology, 2017 525: p. 2287–2309. [PubMed: 28340519]
54. Paxinos G and Franklin KBJ, The mouse brain in stereotaxic coordinates Cambridge: MA, Academic Press, 2008 4th ed.: p. 68–86.
55. Sugino Y, et al., Voided stain on paper method for analysis of mouse urination. Neurourol Urodyn, 2008 27(6): p. 548–52. [PubMed: 18551561]
56. Hill WG, et al., Void spot assay: recommendations on the use of a simple micturition assay for mice. Am J Physiol Renal Physiol, 2018 315: p. F1422–F1429. [PubMed: 30156116]
57. Bjorling DE, et al., Evaluation of voiding assays in mice: impact of genetic strains and sex. Am J Physiol. Renal Physiol, 2015 308(12): p. F1369–1378. [PubMed: 25904700]
58. Chen Y, et al., Sensory detection of food rapidly modulates arcuate feeding circuits. Cell Reports, 2015 160: p. 829–841.
59. Pedersen NP, et al., Supramammillary glutamate neurons are a key node of the arousal system. Nature Communications, 2017 8(1405): p. 1–16.
60. Hull C, Adesnik H, and Scanziani M.a., Neocortical Disynaptic Inhibition Requires Somatodendritic Integration in Interneurons. The Journal of Neuroscience, 2009 29(28): p. 8991–8995. [PubMed: 19605636]
61. Petreanu L, et al., The subcellular organization of neocortical excitatory connections. Nature, 2009 457: p. 1142–5. [PubMed: 19151697]
62. Venner A, et al., A Novel Population of Wake-Promoting GABAergic Neurons in the Ventral Lateral Hypothalamus. Current Biology, 2016 26: p. 2137–2143. [PubMed: 27426511]
63. Krashes MJ, et al., An excitatory paraventricular nucleus to AgRP neuron circuit that drives hunger. Nature, 2014 507(7491): p. 238–42. [PubMed: 24487620]
64. Vong L, et al., Leptin Action on GABAergic Neurons Prevents Obesity and Reduces Inhibitory Tone to POMC Neurons. Neuron, 2011 71: p. 142–154. [PubMed: 21745644]
65. Schneider CA, Rasband WS, and Eliceiri KW, NIH image to imageJ: 25 years of image analysis. nat methods, 2012 9(7): p. 671–675. [PubMed: 22930834]

Highlights:

- *In vivo* neuroscience techniques and thermography combined to study urinary continence
- PAG and LHA neurons provide direct excitatory innervation of Barrington's nucleus
- Optogenetic stimulation of neural afferents leads to different void behavior sequence
- The glutamatergic Bar population is necessary and sufficient for micturition behavior

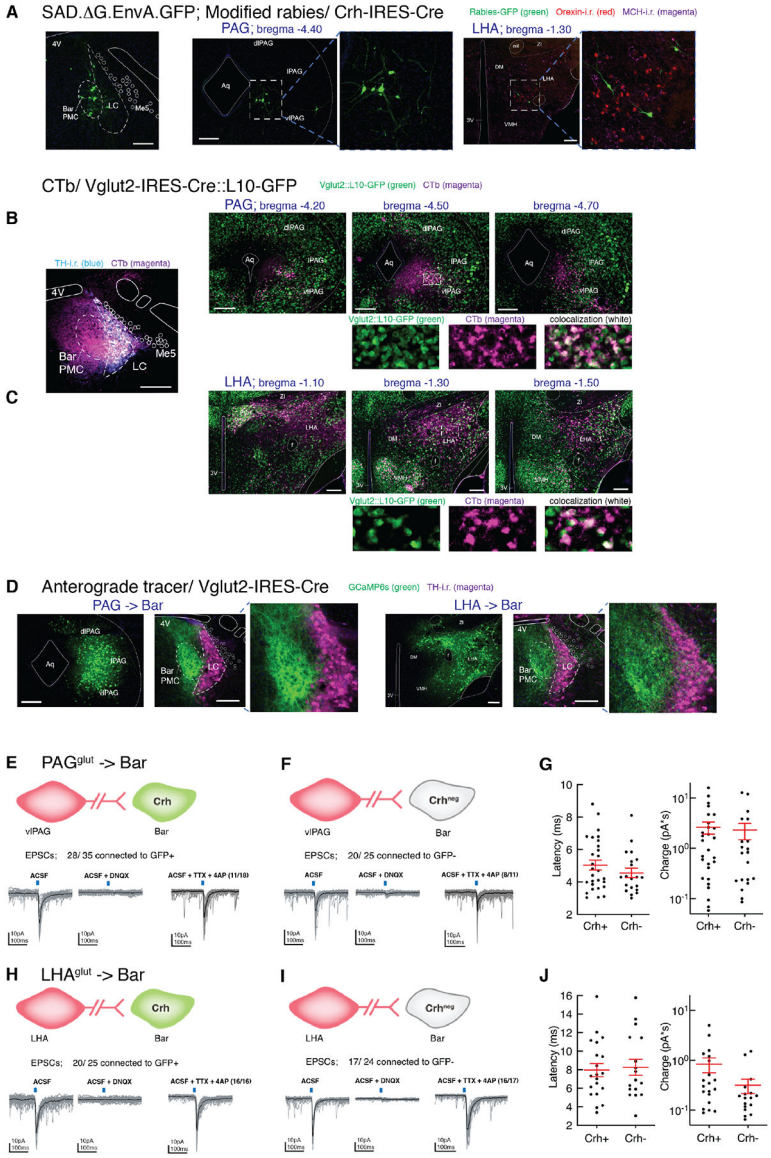

Figure 1. Excitatory neurons in PAG and LHA send axonal projections to soma and dendrites of neurons in Barrington's nucleus and are functionally connected

A) Rabies-eGFP transduced neurons in vlPAG or LHA in a *Crh-IRES-Cre* mouse, with MCH-i.r. labeled neurons shown in magenta and orexin-i.r. labeled neurons in red.

B, C) CTb-labeled neurons (magenta) in PAG (**B**) or LHA (**C**) in *Vglut2-IRES-Cre*::*L10-GFP* (green) reporter mice. Double-labeled neurons appear in white. Shown are the structures at 3 consecutive anterior to posterior levels. Below B' and B" are magnifications of the white boxed region.

D) Anterograde tracer GCaMP6s-labeled (green) axon terminals from transduced neurons in vlPAG or LHA (left images) in *Vglut2-IRES-Cre* mice, and TH-i.r. labeled neurons (magenta) at the level of the PMC (right images). Axons from LHA^{Vglut2} neurons to Bar project to the extensive dendritic arbor of $Bar^{Crh/Vglut2}$ neurons and to the core of Bar. By contrast, axon terminals from PAG^{Vglut2} terminate more densely over the core of Bar and the dorsal dendrites.

E, F, H, I) *In vitro* photostimulation of the vlPAG or LHA input to Bar excites both $Bar^{Crh/Vglut2}$ and $Bar^{Crh\text{-}negative}$ neurons (n = 12 mice and 89 cells, n = 7 mice and 82 cells respectively, 30 light-evoked EPSCs in gray and average light-evoked EPSC in black). In another set of neurons, photostimulation of the vlPAG or LHA input induced light-evoked AMPA receptor mediated EPSCs in $Bar^{Crh/Vglut2}$ and $Bar^{Crh\text{-}negative}$ neurons that were maintained in TTX, in $Bar^{Crh/Vglut2}$ (n = 18 and 16 cells) and $Bar^{Crh\text{-}negative}$ neurons (n = 11 cells and 17 cells). See also Figure S1A,B.

G) From PAG input; light-evoked EPSC latency (left) and charge (right) in 28 $Bar^{Crh/Vglut2}$ and 20 $Bar^{Crh\text{-}negative}$ neurons.

J) From LHA input; light-evoked EPSC latency (left) and charge (right) in 20 $Bar^{Crh/Vglut2}$ and 17 $Bar^{Crh\text{-}negative}$ neurons.

Scale bar is 200 μm. Blue bars at the top of the recording traces indicate 10 ms blue light pulse stimulation. Group data are presented as mean ± s.e.m. *Abbreviations: 3V, 3rd ventricle; 4V, 4th ventricle; Aq, Aqueduct; Bar, Barrington's nucleus; CTb, cholera toxin b; DM, dorsomedial hypothalamic nucleus; mt, mammillothalamic tract; i.r., immunoreactive; LC, locus coeruleus; LHA, lateral hypothalamic area; MCH, melanin concentrating hormone; Me5, trigeminal mesencephalic nucleus; PAG, periaqueductal gray; PMC, pontine micturition center; scp, superior cerebellar peduncle; TH, tyrosine hydroxylase; VMH, ventromedial hypothalamic nucleus; ZI, zona incerta*.

See also Figure S1.

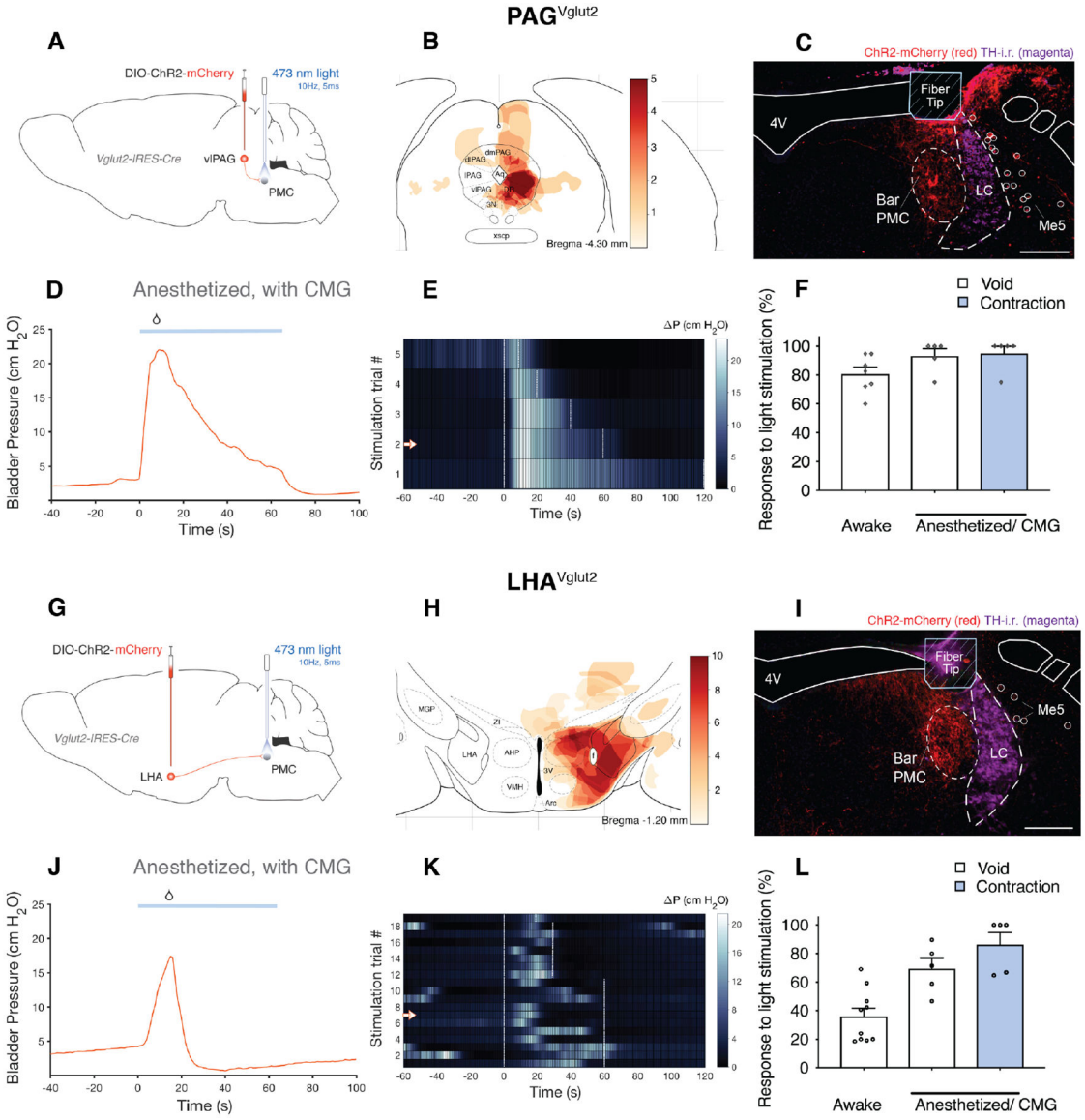

Figure 2. Optogenetic activation of excitatory Bar afferents leads to void responses and increased bladder pressure

Effects of optogenetically activating vlPAG$^{Vglut2 \rightarrow Bar}$ or LHA$^{Vglut2 \rightarrow Bar}$ axon terminals on micturition behavior in awake and urethane anesthetized mice.

A, G) Schematic of Cre-dependent ChR2.mCherry construct and viral targeting unilateral to the PAG or the LHA in *Vglut2-IRES-Cre* mice with optical fiber directed above the ipsilateral Bar.

B) Weighted heatmap, according to behavior response, showing overlapping regions of transduced neurons from 5 mice in which stimulating vlPAG$^{Vglut2 \rightarrow Bar}$ axon terminals unilaterally, evoked void responses.

C, I) DIO.ChR2.mCherry expressing vlPAG$^{Vglut2 \rightarrow Bar}$ or LHA$^{Vglut2 \rightarrow Bar}$ axon terminals (red), optical fiber placement and TH-i.r. labeled neurons (magenta) at the level of the PMC.

D, J) A representative CMG bladder pressure trace under anesthesia, before, during and after optogenetic stimulation (blue line; 10 Hz, 5 ms pulses) in a *Vglut2-IRES-Cre* mouse with DIO.ChR2 targeted to the vlPAG or to the LHA. See also Figure S2C,D.

E, K) Representative heatmap showing Δ pressure before, during and after optogenetic stimulation from one mouse (stimulus onset at time = 0s). Single stimulation trials are sorted by stimulation duration (white dashed lines). Stimulation trial marked by arrow in heatmap corresponds to CMG trace (**D, J**).

F) Likelihood of a micturition event following optogenetic stimulation of $vlPAG^{Vglut2 \rightarrow Bar}$ axon terminals in awake mice ('Awake'; n = 7 mice, 150 stimulations) and in anesthetized mice ('Anesthetized/CMG'; n = 5 mice, 31 stimulations).

H) Weighted heatmap as in B, from 10 mice in which stimulating $LHA^{Vglut2 \rightarrow Bar}$ axon terminals unilaterally evoked void responses.

L) Likelihood of a micturition event following optogenetic stimulation of $LHA^{Vglut2 \rightarrow Bar}$ axon terminals in awake mice ('Awake'; n = 10 mice, 285 stimulations) and in anesthetized mice ('Anesthetized/CMG'; n = 5 mice, 87 stimulations). Data are represented as population mean ± s.e.m.

Scale bar is 200 μm. Droplet icon indicates voiding contraction leading to a void.

Abbreviations: 4V, 4^{th} ventricle; Bar, Barrington's Nucleus; CMG, cystometrogram; ChR2, Channelrhodopsin2; i.r., immunoreactive; LC, locus coeruleus; LHA, lateral hypothalamic area; Me5, trigeminal mesencephalic nucleus; PAG, periaqueductal gray; PMC, pontine micturition center; TH, tyrosine hydroxylase; vl, ventrolateral.

See also Figure S2.

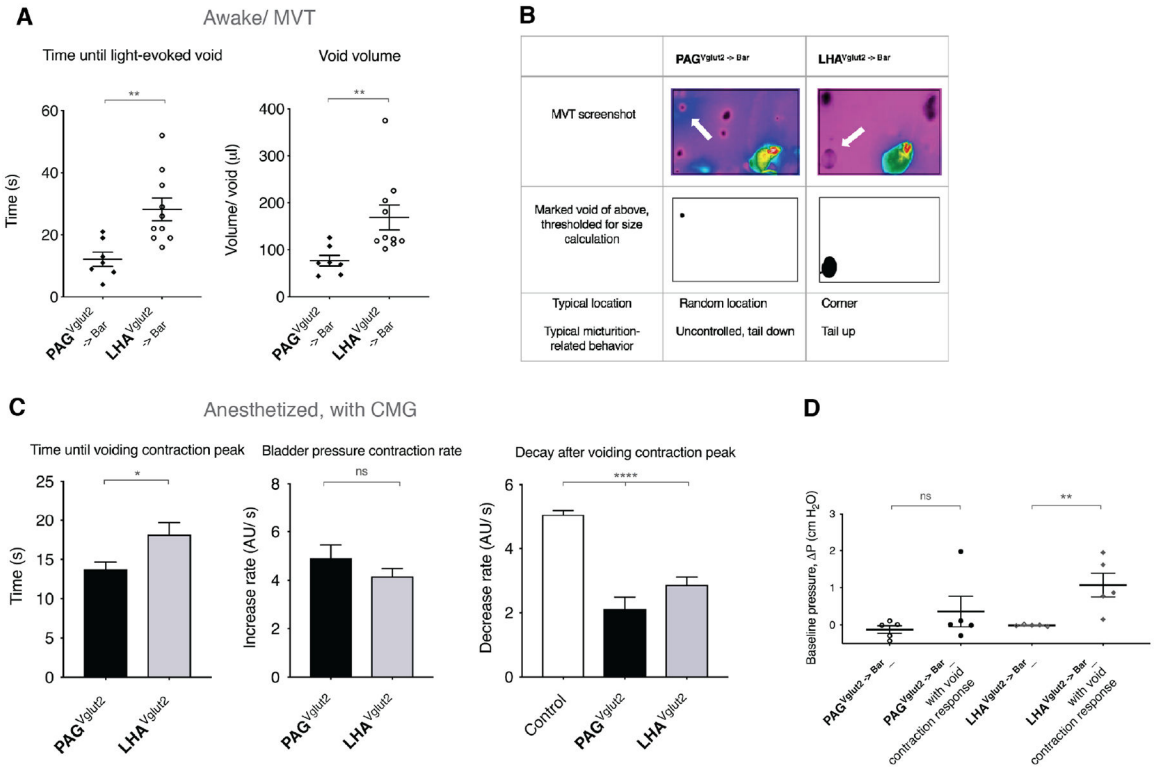

Figure 3. Optogenetic stimulation of axon terminals in Bar causes instant urinary incontinence or voiding in a designated place

A) Averaged time until a light-evoked void from stimulation start (left graph), for $PAG^{Vglut2 \text{ -> } Bar}$ and $LHA^{Vglut2 \text{ -> } Bar}$ in awake mice. Unpaired t-test with Welch's correction; **, p = 0.0022. Averaged volume per void of a light-evoked void (right graph), for $PAG^{Vglut2 \text{ -> } Bar}$ and $LHA^{Vglut2 \text{ -> } Bar}$. Unpaired t-test with Welch's correction; **, p = 0.0080.

Data are presented as mean ± s.e.m. in individual mice. PAG^{Vglut2}, 120 events in 7 mice; LHA^{Vglut2}, 101 events in 10 mice. See also Figure S3A.

B) Screenshot images of a video thermography, awake behavior recording. Arrows point to a light-evoked void during a stimulation trial. Below the screenshot is the indicated void of above, thresholded for void volume calculation. The lower row: typical location of a light-evoked void per condition, and typical behavior observed.

C) Left panel: Time until voiding contraction peak with light-stimulation under anesthesia. Unpaired t test with Welch's correction; *, p = 0.0146.

Middle panel: Bladder pressure contraction rate from start of light stimulation until voiding contraction peak. Unpaired t test with Welch's correction; ns.

Right panel: Pressure decrease in 15 seconds post light-evoked void contraction peak. One-way ANOVA; ****, p < 0.0001, followed by Dunnett's test for multiple comparisons; ****, p < 0.0001 for $PAG^{Vglut2 \text{ -> } Bar}$ and $LHA^{Vglut2 \text{ -> } Bar}$ vs. control. $Bar^{Control}$, n = 29 spontaneous void events without light stimulation in 3 mice; $PAG^{Vglut2 \text{ -> } Bar}$, 25 light-evoked void events in 4 mice; $LHA^{Vglut2 \text{ -> } Bar}$, 51 light-evoked void events in 5 mice. Data are presented as sample mean ± s.e.m. See also Figure S3C.

D) Baseline bladder pressure prior to optogenetic stimulation, all responses versus void contraction responses only. Data are presented as population mean ± s.e.m., n = 5 mice (35 events). Mann-Whitney test; ns p = 0.44 between all responses and void responses for $PAG^{Vglut2 \rightarrow Bar}$ axon terminal stimulation. n = 5 mice (87 events), **, p = 0.0079 all responses versus void responses for $LHA^{Vglut2 \rightarrow Bar}$ axon terminal stimulation.
Abbreviations: Bar, Barrington's nucleus; CMG, cystometrogram; ns, not significant; LHA, lateral hypothalamic area; MVT, Micturition Video Thermography; PAG, periaqueductal gray.
See also Figure S3.

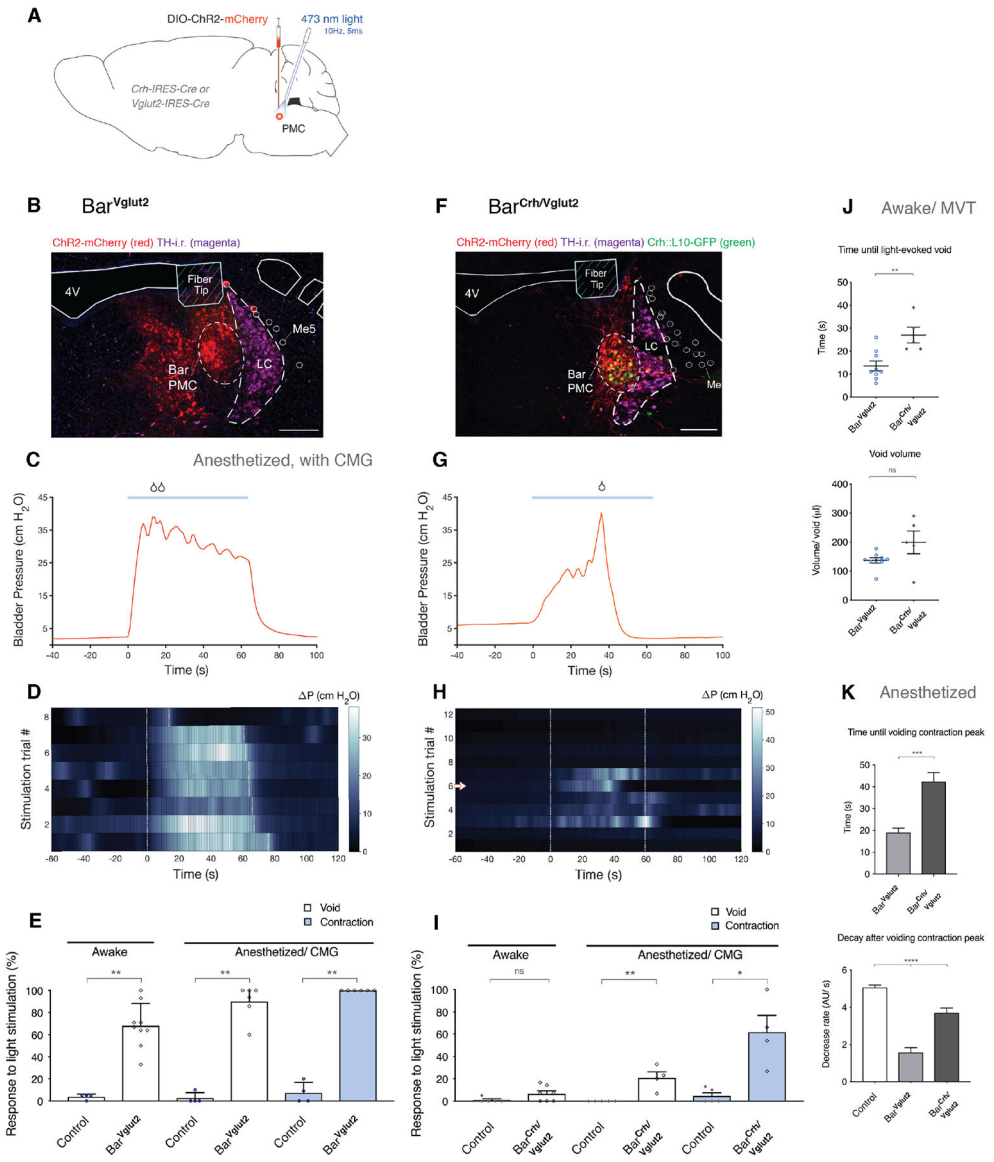

Figure 4. Direct optogenetic activation of neuron subpopulations in Bar triggers micturition behavior

Effects of optogenetic activation of Bar^{Vglut2} or Bar$^{Crh/Vglut2}$ neurons on micturition behavior in awake and anesthetized mice.

A) Schematic of Cre-dependent ChR2.mCherry construct and viral targeting unilateral to Bar in a *Crh-IRES-Cre or Vglut2-IRES-Cre (::L10-GFP)* mouse.

B, F) DIO.ChR2.mCherry transduced neurons (red), Crh-expressing neurons (green), optical fiber placement and TH-i.r. labeled neurons (magenta) at the level of the PMC.

C, G) A representative cystometry (CMG) bladder pressure trace, before, during and after optogenetic stimulation (blue line; 10 Hz, 5 ms pulses) in an anesthetized V*glut2-IRES-Cre* or *Crh-IRES-Cre* mouse with DIO.ChR2 injected in Bar. See also Figure S4D.

D, H) Heatmap showing ΔP before, during and after optogenetic stimulation (stimulus onset at time = 0s) from one representative mouse.

H) Stimulation trial marked by arrow in heatmap corresponds to CMG trace (**G**).

E) Likelihood of a micturition event following optogenetic stimulation of Bar^{Vglut2} neurons in awake mice ('Awake'; n = 9 mice, 122 stimulations) and in anesthetized mice ('Anesthetized/CMG'; n = 6 mice, 43 stimulations), versus control *Vglut2-IRES-Cre* mice with AAV.DIO.mCherry injected in Bar ('Awake'; n = 4 mice, 88 stimulations, and 'Anesthetized/CMG'; n = 4 mice, 43 stimulations). Mann-Whitney test; **, p = 0.0028; for 'void responses' in awake mice, **, p = 0.0095 and **, p = 0.0048 for 'void responses' and 'contractions' under anesthesia respectively.

I) Likelihood of a micturition event following optogenetic stimulation of $Bar^{Crh/Vglut2}$ neurons in awake mice ('Awake'; n = 7 mice, 82 stimulations) and in anesthetized mice ('Anesthetized/CMG'; n = 4 mice, 45 stimulations), versus control *Crh-IRES-Cre* mice with AAV.DIO.mCherry injected in Bar ('Awake'; n = 5 mice, 91 stimulations, and 'Anesthetized/CMG'; n = 5 mice, 76 stimulations). Mann-Whitney test; p = ns; for 'void responses' in awake mice, **, p = 0.0079 and *, p = 0.0159 for 'void responses' and 'contractions' under anesthesia respectively.

J) Upper graph: Averaged time until a light-evoked void from stimulation start, for Bar^{Vglut2} and $Bar^{Crh/Vglut2}$ in awake mice. Mann-Whitney test; **, p = 0.0060.

Lower graph: Averaged volume per void of a light-evoked void, for Bar^{Vglut2} and $Bar^{Crh/Vglut2}$ in awake mice; ns. Data are presented as mean ± s.e.m. in individual mice. Bar^{Vglut2}, 85 events in 9 mice; $Bar^{Crh/Vglut2}$, 5 events in 4 mice.

K) Upper graph: Time until voiding contraction peak with light-stimulation under anesthesia. Unpaired t test with Welch's correction; ***, p = 0.0002.

Lower graph: Pressure decrease in 15 seconds post light-evoked void contraction peak. One-way ANOVA; ****, p < 0.0001, followed by Dunnett's test for multiple comparisons; ****, p < 0.0001 and *, p = 0.0121 for Bar^{Vglut2} and $Bar^{Crh/Vglut2}$ respectively vs. control. Data are presented as sample mean ± s.e.m., $Bar^{Control}$, n = 29 spontaneous void events without light stimulation in 3 mice; Bar^{Vglut2}, 31 light-evoked void events in 6 mice; $Bar^{Crh/Vglut2}$, 7 light-evoked void events in 3 mice.

Single stimulation trials are sorted by stimulation duration (white dashed lines). Scale bar is 200 μm. Droplet icon indicates voiding contraction leading to a void. *Abbreviations: 4V, 4th ventricle; Bar, Barrington's Nucleus; CMG, cystometrogram; ChR2, Channelrhodopsin2; i.r., immunoreactive; MVT, Micturition Video Thermography; LC, locus coeruleus; Me5; trigeminal mesencephalic nucleus; ns, not significant; PMC, pontine micturition center; TH, tyrosine hydroxylase*.

See also Figure S4.

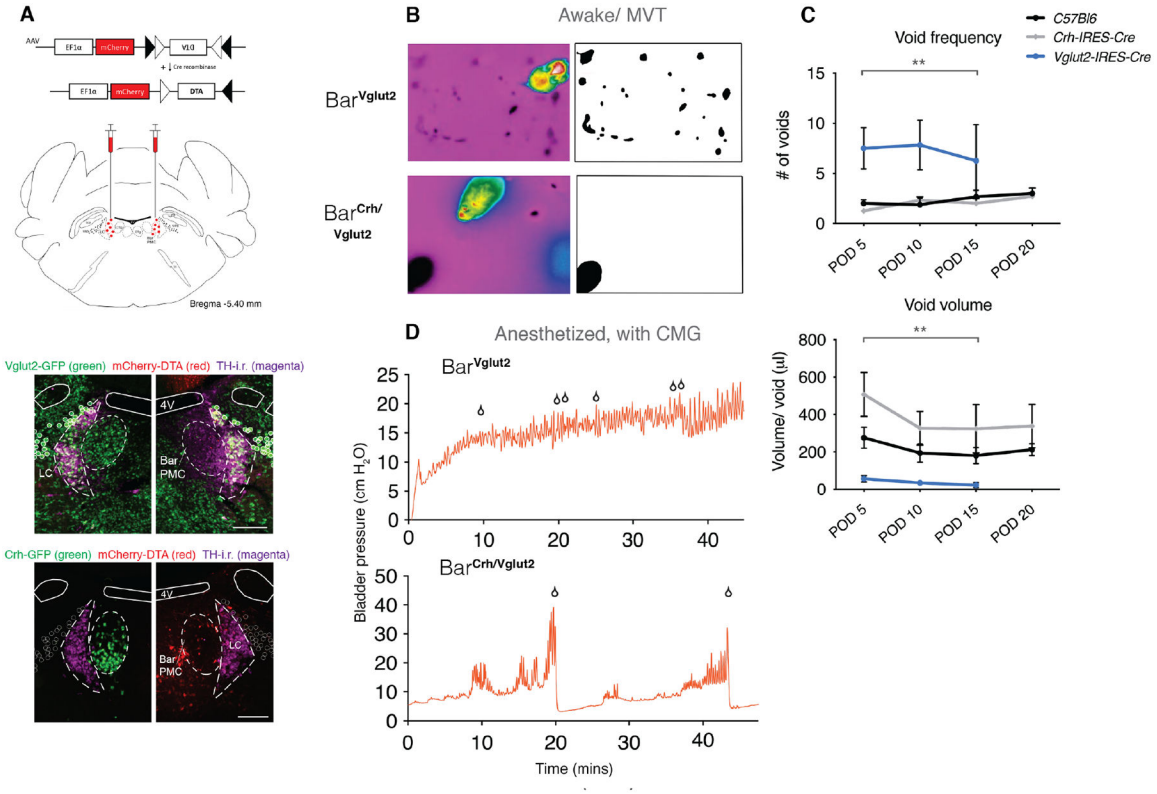

Figure 5. Selective ablation of glutamatergic or glutamatergic-Crh+ Bar neurons causes retention or delays voiding contractions

A) Schematic of Cre-dependent diphtheria toxin subunit A (DTA) construct and viral targeting bilaterally to Bar. mCherry is located upstream of the DIO-DTA sequence, thus labeling non-Cre expressing transduced neurons.

Lower panel: Upper image, right side: DIO-DTA expression in transduced Bar^{Vglut2} neurons and uninjected Bar^{Vglut2} (GFP+) neurons in the control side (up left), TH-i.r. labeled neurons shown in magenta. Unilateral selective neuronal ablation of GFP+ $Bar^{Crh/Vglut2}$ neurons (lower image, right side) and remaining $Bar^{Crh/Vglut2}$ (GFP+) neurons in the uninjected side (down left). See also Figure S5A–C.

B) Representative thermal camera screenshots of the voiding pattern after 2 hours awake thermography recording, from a *Vglut2-IRES-Cre* mouse injected with DIO-DTA (upper panel), and a *Crh-IRES-Cre* mouse injected with DIO-DTA (lower panel) at POD 15. Next to the screenshots are images with thresholding applied to the void spot(s) for void size calculation.

C) Frequency of voiding (upper graph) and volume per void (lower graph) during a 2-hour video thermography awake behavior recording on POD 5, 10, 15 or 20. Data is represented as population mean ± s.e.m. for *C57Bl6/J* ($Bar^{Control}$, n = 9 mice), *Crh-IRES-Cre* ($Bar^{Crh/Vglut2}$, n = 7 mice) and *Vglut2-IRES-Cre* (Bar^{Vglut2}, n = 4 mice) injected bilaterally with DIO-DTA. RM one-way ANOVA; **, p = 0.0013 for frequency, with Dunnett's multiple comparisons test; ns control vs $Bar^{Crh/Vglut2}$, **, p = 0.0017 control vs. Bar^{Vglut2}. RM one-way ANOVA; **, p = 0.0018 for voided volume, with Dunnett's multiple comparisons test; *, p = 0.0169 and *, p = 0.0139 for control vs $Bar^{Crh/Vglut2}$ and Bar^{Vglut2}

respectively. See also Figure S5E,F. Some *Vglut2-IRES-Cre* mice became moribund before POD 20.

D) An example of a CMG bladder pressure trace in an anesthetized *Vglut2-IRES-Cre* (upper panel) and a representative CMG bladder trace in an anesthetized *Crh-IRES-Cre* mouse (lower panel), injected with DIO-DTA in Bar. See also Figure S5G.

Scale bar is 200 μm. Droplet icon indicates urine drops or voiding contraction leading to a void. *Abbreviations: 4V, 4th ventricle; Bar, Barrington's Nucleus; CMG, cystometrogram; DTA, diphtheria toxin A; i.r., immunoreactive; MVT, Micturition Video Thermography; LC, locus coeruleus; ns, not significant; PMC, pontine micturition center; POD, post-operative day; TH, tyrosine hydroxylase*. See also Figure S5.

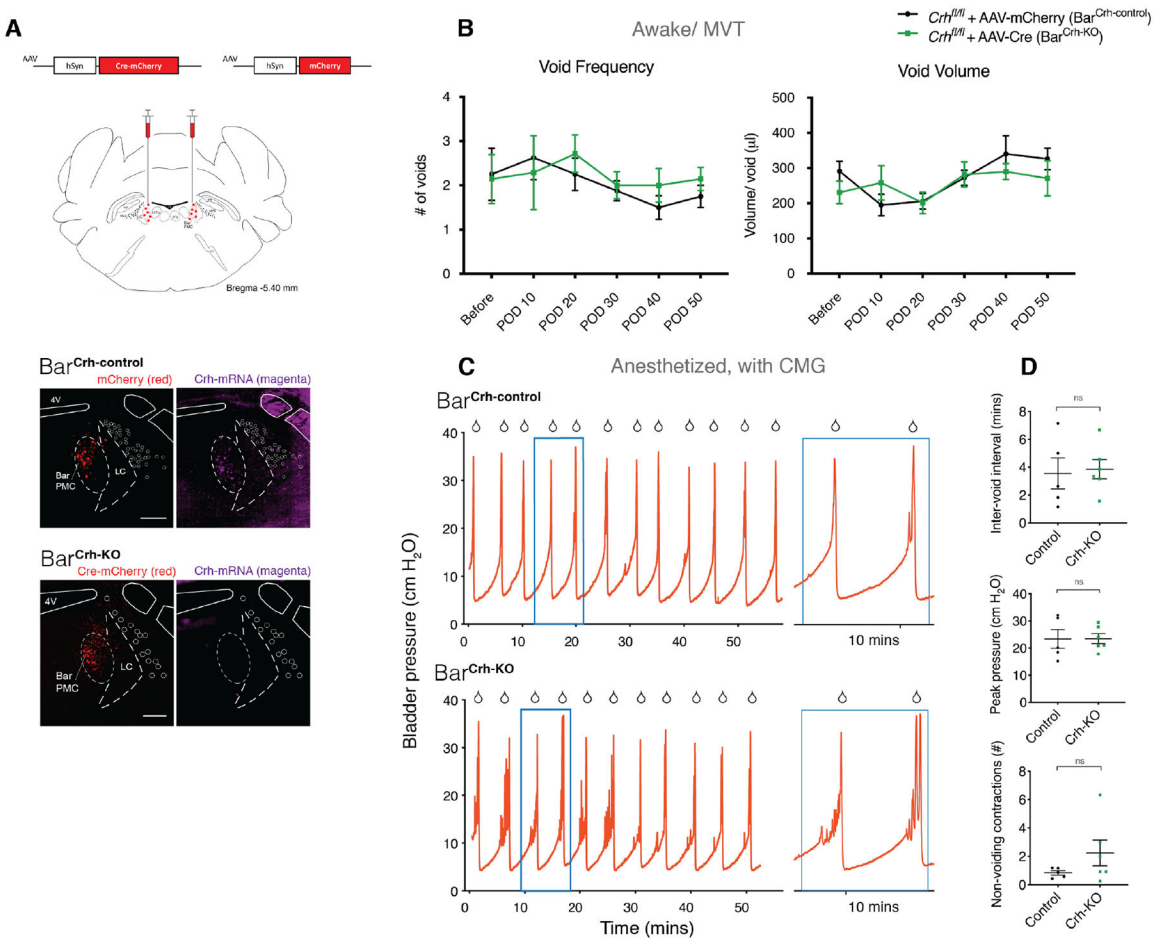

Figure 6. Deleting Crh from Bar neurons does not affect voiding behavior significantly

Effects of Crh knockout (KO) by AAV.Cre injection targeted to Bar in adult floxed *Crh* (*Crh*$^{fl/fl}$) mice. **A**) Schematic of AAV.Cre.mCherry or AAV.mCherry construct and viral targeting bilateral to Bar in *Crh*$^{fl/fl}$ mice. Lower panel: Validation of Crh KO with in situ hybridization. Upper panel: AAV.mCherry injected in Crh$^{fl/fl}$ mice; Bar$^{Crh\text{-}control}$, mCherry is labeled in red and mRNA for Crh in magenta.

Lower panel: AAV.Cre.mCherry injected in Crh$^{fl/fl}$ mice; Bar$^{Crh\text{-}KO}$, mCherry is labeled in red and Crh mRNA in magenta. See also Figure S6A,B.

B) Group data showing void frequency (left graph), and volume per void (right) over 50 days from 2-hour MVT trials, following AAV.mCherry (Bar$^{Crh\text{-}control}$) or AAV.Cre (Bar$^{Crh\text{-}KO}$) injection. Data are presented as population mean ± s.e.m., n = 8 mice for Bar$^{Crh\text{-}control}$, n = 7 mice for Bar$^{Crh\text{-}KO}$. Two-way ANOVA with Sidak's multiple comparisons test, ns for any POD (frequency and voided volume).

C) Representative CMG bladder pressure traces from anesthetized *Crh*$^{fl/fl}$ mice injected with AAV.mCherry (upper trace: Bar$^{Crh\text{-}control}$) or AAV.Cre (lower: Bar$^{Crh\text{-}KO}$). Right panels: magnification of the blue boxed portion.

D) Quantitative analysis of CMG traces. Interval between voids (upper graph), amplitude of void contractions (middle), and number of non-voiding contractions per void cycle (lower),

in $Bar^{Crh\text{-}control}$ (n = 5 mice) versus $Bar^{Crh\text{-}KO}$ (n = 6 mice). Mann-Whitney test, ns for any of the three parameters.

Scale bar is 200 μm. Droplet icon indicates voiding contraction leading to a void.

Abbreviations: 4V, 4th ventricle; Bar, Barrington's Nucleus; CMG, cystometrogram; i.r., immunoreactive; KO, knockout; MVT, Micturition Video Thermography; LC, locus coeruleus; ns, not significant; PMC, pontine micturition center; POD, post-operative day.

See also Figure S6.

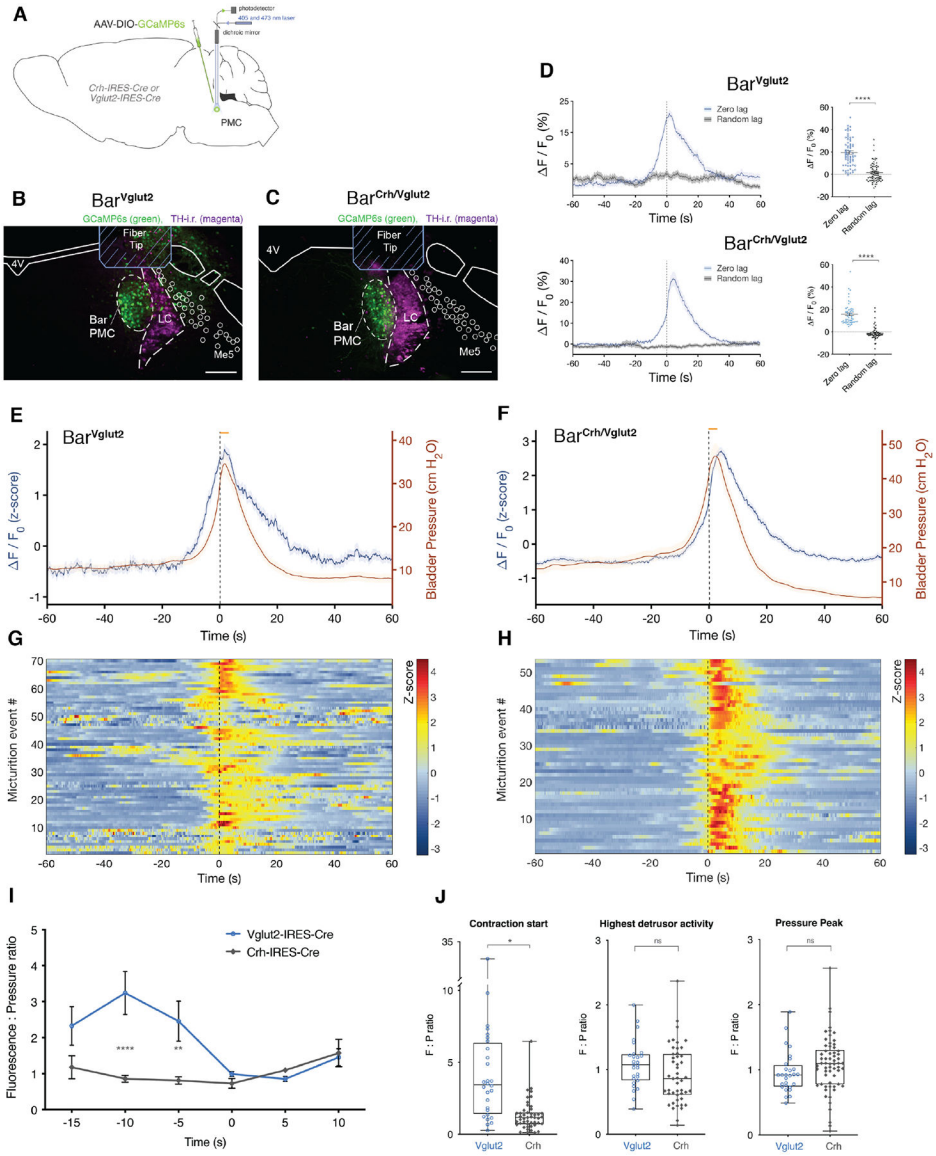

Figure 7. Specific Bar subpopulations have distinct activity patterns related to micturition behavior in awake freely-behaving mice

In vivo fiber photometry of Bar^{Vglut2} and Bar$^{Crh/Vglut2}$ neurons with cystometry in awake mice.

A) Schematic of GCaMP6s construct and viral targeting unilateral to Bar in a *Vglut2-IRES-Cre* or *Crh-IRES-Cre* mouse.

B, C) GCaMP6s transduced neurons (green), optical fiber placement and TH-i.r. labeled neurons (magenta) at the level of Bar in a *Vglut2-IRES-Cre* or a *Crh-IRES-Cre* mouse.

D) Averaged GCaMP6s signal (in blue; $\Delta F/F_0$; zero lag) in Bar^{Vglut2} neurons (upper panel, n = 70) or Bar$^{Crh/Vglut2}$ neurons (lower panel, n = 53) with micturition events, or at random timepoints (in black; $\Delta F/F_0$; random lag). Unpaired t test with Welch's correction; ****, $p < 0.0001$.

E) Averaged CMG trace (in red; ΔP), and GCaMP6s signal (in blue; $\Delta F/F_0$ converted to a z-score) in Bar^{Vglut2} neurons. Data are presented as sample mean ± s.e.m., n = 70 events from four mice. The shade in the graph represents the standard error of the mean.

F) Averaged CMG trace (in red; ΔP), and GCaMP6s signal (in blue; $\Delta F/F_0$ converted to a z-score) in $Bar^{Crh/Vglut2}$ neurons. Data are presented as sample mean ± s.e.m., n = 53 events from four mice.

G, H) Heatmap showing GCaMP6s signal ($\Delta F/F_0$) before, during and after individual micturition events for Bar^{Vglut2} (**G**) or $Bar^{Crh/Vglut2}$ neurons (**H**).

I) Fluorescence to pressure ratio, before and after a micturition event, in *Vglut2-IRES-Cre* mice (n = 4 mice) and *Crh-IRES-Cre* (n = 4 mice). Two-way ANOVA followed by Sidak's multiple comparisons test; at −10s, **** $p < 0.0001$, at −5s, ** $p = 0.0068$. Data are presented as population mean ± s.e.m.

J) Fluorescence to pressure ratio for timepoints 'contraction start' (t = −10s), for 'highest detrusor activity' (t = 0s) and for void contraction 'pressure peak' (t = 5s) in *Vglut2-IRES-Cre* mice (n = 4 mice) and *Crh-IRES-Cre* (n = 4 mice). Mann-Whitney test at 'contraction start', * $p = 0.0286$. Data are presented as population medians, with min to max values of the first 7 events for each mouse.

Scale bars 200 μm. The orange bar represents the approximate void start and duration. Black line, t = 0; highest detrusor activity. *Abbreviations: 4V, 4th ventricle; Bar, Barrington's Nucleus; i.r., immunoreactive; LC, locus coeruleus; Me5, trigeminal mesencephalic nucleus; PMC, pontine micturition center; TH, tyrosine hydroxylase*.

KEY RESOURCES TABLE

REAGENT or RESOURCE	SOURCE	IDENTIFIER
Antibodies		
CTb	List Biological,	goat polyclonal, Cat.# 703, lot# 115037, RRID: AB_10013220
dsRed	Clontech,	rabbit polyclonal, Cat.# 632496, RRID: AB_10015246
mCherry	Life Sciences,	rat monoclonal, Cat.# M11217, RRID: AB_2536611
GFP	Invitrogen,	chicken polyclonal, Cat.# A10262, RRID: AB_2534023
TH	Millipore,	mouse monoclonal, Cat.# 657010, RRID: AB_212601
Mouse, goat, rabbit or rat	Invitrogen,	Alexa fluorophore −488, −594 or −647, Cat.# A21203, A-21202, A-31571, A-11058, A-11055, A-21447, A-21207, A-21206, A-31573, A-21208, A-21209
Bacterial and Virus Strains		
AAV8.hSyn.DIO.hM3Dq.mCherry	University of North Carolina Vector Core	
AAV9.CBA.Flex.rev.ChR2(H134R).mCherry	University of Pennsylvania Vector Core	Addgene #18916
AAV8.DIO.mCherry	University of North Carolina Vector Core	Cat.# 4981
AAV1.hSyn.Flex.GCaMP6s	University of Pennsylvania Vector Core	Addgene #100845
AAV9.CAG.ChR2(H134R).mCherry	University of Pennsylvania Vector Core	Addgene #20928
AAV10.EF1a.mCherry.DIO.dtA		P. Fuller, M. Lazerus, Beth Israel Deaconess Medical Center
AAV8.hSyn.Cre.mCherry	University of North Carolina Vector Core	
AAV8.hSyn.mCherry	University of North Carolina Vector Core	
AAV8.DIO.Syp.YFP	Virovek	
AAV8.CAG.Flex.RG	Stanford Medicine, Gene Vector and Virus Core	GVVC-AAV-59
AAV8.EF1α.Flex.TVA.mCherry	University of North Carolina Vector Core	
SAD.ΔG.EnvA.GFP	Salk Institute for Biological Studies, Viral Vector Core	Cat.# 32635
Biological Samples		
Chemicals, Peptides, and Recombinant Proteins		

REAGENT or RESOURCE	SOURCE	IDENTIFIER
Critical Commercial Assays		
Deposited Data		
Experimental Models: Cell Lines		
Experimental Models: Organisms/Strains		
Oligonucleotides		
Recombinant DNA		
Software and Algorithms		
ImageJ	[65]	https://imagej.nih.gov/ij/
LabChart		National Instruments
Prism 7 software	GraphPad (San Diego, CA, USA)	https://www.graphpad.com
Microsoft Excel	Microsoft	
Adobe Illustrator	Adobe	https://www.adobe.com
Doric customized scripts	Doric Lenses	http://doriclenses.com
Flir, ResearchIR	Flir	https://www.flir.com
Adobe Photoshop	Adobe	https://www.adobe.com
Matlab	Mathworks	https://matworks.com
Matlab custom scripts	This paper	Available on request
Python custom scripts	[62]	NA
VLC media player	VideoLAN	http://www.videolan.org
OlyVIA software	Olympus	https://www.olympus-lifescience.com
VS-ASW software	Olympus	https://www.olympus-lifescience.com
Arduino Software, Sketch	Arduino cc	https://www.arduino.cc
Clampfit 10	Molecular Devices	https://www.moleculardevices.com
Mini Analysis 6 software	Synaptosoft	http://www.synaptosoft.com/MiniAnalysis/

REAGENT or RESOURCE	SOURCE	IDENTIFIER
Other		
Other		